A Model Describing the Inactivation of Factor Va by APC: Bond Cleavage, Fragment Dissociation, and Product Inhibition†

Matthew F. Hockin, Kevin M. Cawthern, Michael Kalafatis,‡ and Kenneth G. Mann*

Department of Biochemistry, The University of Vermont, College of Medicine, Burlington, Vermont 05405

Received August 17, 1998; Revised Manuscript Received March 18, 1999

ABSTRACT: The inactivation of factor Va is a complex process which includes bond cleavage (at three sites) and dissociation of the $A2_N$·$A2_C$ peptides, with intermediate activity in each species. Quantitation of the functional consequences of each step in the reaction has allowed for understanding of the presentation of disease in individuals possessing the factor V polymorphism factor V^{LEIDEN}. APC cleavage of membrane-bound bovine factor Va (Arg^{306}, Arg^{505}, Arg^{662}) leads to the dissociation of fragments of the A2 domain, residues 307−713 ($A2_N$·$A2_C$ + $A2_{C-peptide}$), leaving behind the membrane-bound A1·LC species. Evaluation of the dissociation process by light scattering yields invariant mass loss estimates as a function of APC concentration. The rate constant for A2 fragment dissociation varies with [APC], reaching a maximal value of $k = 0.028$ s^{-1}, the unimolecular rate constant for A2 domain fragment dissociation. The APC binding site resides in the factor Va light chain (LC) ($K_d = 7$ nM), suggesting that the membrane-bound LC·A1 product would act to sequester APC. This inhibitory interaction (LC·A1·APC) is demonstrated to exist with either purified factor Va LC or the products of factor Va inactivation. Utilizing these experimental data and the reported rates of bond cleavage, binding constants, and product activity values for factor Va partial inactivation products, a model is developed which describes factor Va inactivation and accounts for the defect in factor V^{LEIDEN}. The model accurately predicts the rates of inactivation of factor Va and factor Va^{LEIDEN}, and the effect of product inhibition. Modeled reaction progress diagrams and activity profiles (from either factor Va or factor Va^{LEIDEN}) are coincident with experimentally derived data, providing a mechanistic and kinetic explanation for all steps in the inactivation of normal factor Va and the pathology associated with factor V^{LEIDEN}.

The regulation of factor Va activity is a central event in hemostasis (*2*, *3*). The expression of factor Va cofactor activity through activation of the procofactor factor V by thrombin generates one of the necessary components of the prothrombinase complex (*4*−*7*). Factor Va acts as a membrane receptor for factor Xa formed by either the intrinsic or the extrinsic tenases (*8*, *9*). The net effect of the interaction is to recruit factor Xa to the membrane surface (*10*, *11*) and to modulate positively the efficiency of factor Xa. The combination of these functions increases the rate of prothrombin activation by 5 orders of magnitude (*4*). Factor Va activity is regulated by proteolytic inactivation by activated protein C (APC) (*1*, *12*). APC is formed through a thrombin feedback loop wherein the specificity of thrombin is modulated from procoagulant to anticoagulant through binding to its endothelial cell associated cofactor thrombomodulin; once bound, thrombin/thrombomodulin specifically and rapidly activates protein C (*13*−*15*).

The inactivation of bovine factor Va by APC is a complex proteolytic process involving four cleavages (at $Arg^{306,505,662,1752/3}$)[3] that yield a factor Va molecule which possesses no cofactor activity and is comprised of six peptide chains: 1−306 (A1), 307−505 ($A2_N$), 506−662 ($A2_C$), 663−713 ($A2_{C-peptide}$), 1545−1752(3) (LC_{NH2}), 1753(4)−2096 (LC_{COOH}).

The kinetics of human factor Va inactivation have been studied by initial rate approximations (*16*), progress curve analysis based upon simple kinetic models (*17*), densitometry of product formation (*17*, *18*), natural cleavage site mutants

† This work was supported in part through National Institutes of Health (NIH) Merit Award HL-34575 to K.G.M. Portions of this work were presented in abstract form at the American Society of Hematology Conference, San Diego, CA, Dec 5−9 (*65*).

* To whom correspondence should be addressed. E-mail: kmann@protein.med.uvm.edu.

‡ Present address: Department of Chemistry, Science Building, 2351 Euclid Ave., Cleveland State University, Cleveland, OH 44115. Telephone: (216) 687-2460. Fax: (216) 687-9298. E-mail: m.kalafatis@popmail.csuohio.edu.

[1] Abbreviations: Va, factor Va; Va_n, factor Va cleaved at site 505 (Va_5), 306 (Va_3), or 662 (Va_6); HC, heavy chain (factor Va); HC_n, heavy chain cleaved at site 505 (HC_5), 306 (HC_3), or 662 (HC_6); LC, light chain (factor Va); PC, protein C; APC, activated protein C; APC_i, active site inhibited activated protein C (DFP); LUV, large unilamellar vesicle(s); SUV, small unilamellar vesicle(s); PC_l, L-α-phosphatidylcholine; PS_l, L-α-phosphatidyl-L-serine; DOPC, 1,2-dioleoyl-*sn*-3-glycerophosphocoline; DOPS, 1,2-dioleoyl-*sn*-3-glycerophospho[L-serine]; DAPA, dansylarginine *N*-(3-ethyl-1,5-pentanediyl)amide; cps, counts per second; θ, fractional saturation of factor Va (% bound); θ', fractional saturation of lipid headgroups (% occupied); υ, partial specific volume; *S*, Svedberg constant; *D*, diffusion coefficient (cm^2/s); L_S, lipid site for Va binding; $[L_s]_t$, molar concentration of total "sites" for Va binding; $[L_t]$, molar concentration of lipid headgroups; K_d, binding constant; *i*, number of sites per phospholipid for Va binding ($1/n$); *n*, stoichiometry in terms of the number of lipids bound per Va ($1/i$).

[2] In the human system, the equivalent bond cleavage sites are Arg^{506}, Arg^{306}, and Arg^{679} (*1*).

[3] Numbering as for the bovine system.

10.1021/bi981966e CCC: $18.00
Published on Web 05/05/1999

(*19*, *20*), and recombinant mutants (*16*). These approaches have led to a family of kinetic constants for individual bond cleavage rates that are in general agreement.

The bovine factor Va molecule is composed of two peptide chains: the heavy chain (1−713) (HC) and the light chain (1546−2183) (LC) (*21*, *22*). Association of the HC and LC is metal ion dependent (*23*) and is characterized by a K_d of 5.9 nM (*24*). The binding interaction between intact factor Va and APC is mediated through the lipid binding LC component of the factor Va molecule and is characterized by a K_d of 7 nM (*25*, *26*). During the inactivation of factor Va which requires the presence of a lipid surface, cleavage occurs in the order 505→306→662 (*12*). Cleavage at Arg^{306} is lipid dependent (*12*, *18*), while cleavage at Arg^{505} is potentiated by a lipid surface (*12*, *18*). Upon cleavage at Arg^{306}, the entire A2 domain of the Arg^{505}-cleaved HC (A1−A2) dissociates from the factor Va molecule as an associated fragment ($A2_N$·$A2_C$) (Arg^{505} is between the α- and β-loops of the HC A2 domain) (*27*). This dissociation event (cleaved A2) generates an inactive factor Va product composed of A1·LC + $A2_N$·$A2_C$. The bovine LC is also cleaved by APC ($Arg^{1752/3}$); however, this cleavage is irrelevant with respect to cofactor activity (*12*, *28*). The LC-mediated binding of APC to factor Va presents an additional complexity in that both the reactant and product are predicted to interact equally with the enzyme (*25*), thus presenting the possibility that a product inhibition mechanism exists and will significantly influence the reaction. As a consequence of these complex interactions, all of which are defined by individual rate processes and equilibrium distributions, the inactivation of factor Va is a complicated problem with respect to both kinetic evaluation of rate constants and deconvolution of mechanistic pathways. To assist in establishing the relevant steps and interactions which define the kinetics of factor Va inactivation, we constructed a mathematical model (*29*−*32*) of factor Va inactivation. The set of kinetic parameters necessary to describe this model is not completely defined for either the human or the bovine system. However, complementary information is available in part for each case, allowing construction of a composite collection of rate constants and binding measurements, which we have assumed to apply equally well to either system. The development of this model system allows predictions to be made based upon a firm kinetic foundation and assists in directing research efforts to better understand factor Va inactivation.

The importance of the proper regulation of the activity of factor Va by APC has been explicitly demonstrated through the severe pathology associated with factor V^{LEIDEN} (*33*, *34*). Factor V^{LEIDEN} is present in 2−4% of the general caucasian population and is a significant risk factor in predicting thrombotic disease and accounts for a significant fraction of the familial thrombosis previously classified as idiopathic (*35*−*37*). Factor V^{LEIDEN} arises from a genetic mutation predicting an amino acid change, Arg^{506}→Gln^{506}, within the factor Va HC (*35*). The elimination of the Arg^{506} cleavage site has been demonstrated to delay the inactivation of factor V^{LEIDEN}, fitting well with the thrombotic pathology observed in these individuals (*17*, *38*). However, there has been significant debate as to the mechanism of normal factor Va inactivation (and thus factor V^{LEIDEN} by extension) regarding the cleavage ordering, and kinetic mechanism. Modeling the inactivation of factor Va^{LEIDEN} demonstrates that the observed APC resistance is due to the kinetic consequences of the elimination of the Arg^{506} cleavage site in a random cleavage reaction and not a function of eliminating the requisite first step of an ordered or sequential reaction.

METHODS

Reagents. L-α-Phosphatidyl-L-serine (bovine brain) (PS_l), L-α-phosphatidylcholine (egg yolk) (PC_l), Tris-base, and Hepes were purchased from Sigma (St. Louis, MO). Synthetic phospholipids, 1,2-dioleoyl-*sn*-3-glycerophosphocholine (DOPC) and 1,2-dioleoyl-*sn*-3-glycerophospho[L-serine] (DOPS), were purchase from Avanti Polar Lipids (Alabaster, AL). Sodium chloride and calcium chloride were purchased from J. T. Baker (NJ). CHELEX resin was purchased from BioRad (Hercules, CA). Sepharose CL-4b resin was purchased from Pharmacia (Piscataway, NJ). Dansylarginine-*N*-(3-ethyl-1,5-pentanediyl)amide (DAPA) and bovine APC were the gifts of Haematologic Technologies (Essex Junction, VT). Bovine factor Va was isolated as previously described (*39*, *40*). Four separate preparations of factor Va were utilized in this work; each preparation was initiated from a pooled plasma (50l) derived from five cows. The M_r 72 000 and 74 000 LC's of factor Va were separated and purified as previously described (*28*, *41*). Active site inhibited APC (APC_I) was prepared by mixing APC (3 μM) with diisopropyl fluorophosphate (1 mM) (DFP) and incubating at 37 °C for 30 min. The residual APC_I activity was assessed in both end point and kinetic analyses using an S-2236 (200 μM), American Diagnostica (Greenwich, CT), chromogenic assay for APC at 10−400 nM. The absence of any measurable rate of hydrolysis was taken to indicate the complete inhibition of APC; plates utilized for these kinetic assays were allowed to incubate in the dark for 3 h and were inspected visually for color change to further confirm the absence of proteolytic activity.

DOPC/DOPS Preparation for Light Scattering Measurements. DOPC/DOPS vesicles were prepared and manipulated at room temperature from 1,2-dioleoyl-*sn*-3-glycerophosphocoline (DOPC) and 1,2-dioleoyl-*sn*-3-glycerophospho-[L-serine] (DOPS) by sonication (*42*) in CHELEX-treated HBS (150 mM NaCl, 20 mM HEPES, pH 7.4) followed by ultracentrifugation at 25 °C (*42*) and gel filtration of the top $^3/_4$ volume from the centrifuge using a Sepharose CL-4b column (300 mm × 22 mm) (*43*, *44*). The lipid vesicle elution profile was monitored by UV absorbance at 240 nm, phosphorus assay (*45*), and light scattering analyses. Fractions from the portion of the chromatogram exhibiting a stable (phosphorus concentration/light scattering) ratio were pooled, and the lipid concentration was quantified by phosphorus assay as described previously (*45*). The pooled vesicles were stored at room temperature (approximately 22 °C) and used within 36 h of preparation for light scattering analyses.

Further characterization of the DOPC/DOPS vesicles with respect to molecular weight and homogeneity was accomplished using analytical ultracentrifugation in a Beckman XL-I (Palo Alto, CA) analytical ultracentrifuge configured with an An50-ti rotor using aluminum-bodied cells housing a double-sector EPON centerpiece and sapphire windows. For molecular weight estimation, the DOPC/DOPS vesicles were spun at 50 000 rpm using a solution volume of 350 μL

and blanked against the same buffer used to gel-filter the DOPC/DOPS vesicles. UV absorbance (240 nM) scans were taken at 5 min intervals over the entire cell length. The software "Svedberg ver 5.01" (©1992−1998 John S. Philo; Amgen, Inc., Thousand Oaks, CA) was used to fit both *S*/*D* (MW) and *S* and *D* independently using a modified Fuji−MacCosham function. This fit was carried out simultaneously over 10 UV data sets, containing the meniscus and entire boundary, spaced equally in time. A partial specific volume, $\bar{v}$, of 0.9885 cm^3/g was used for the DOPC/DOPS vesicles (*43*, *44*). Vesicle homogeneity was further assessed using sedimentation velocity experiments analyzed using the time derivative method according to the software package DC_DT version 3.10s (©1988−1996 Walter F. Stafford; Harvard University, Cambridge, MA) (*46*). The $g(s^*)$ plots (using Δs values of 0.1 s) obtained from the interference optical scans of the entire cell (assembled as described above) at 10 s intervals were compared at different points in the run (meniscus depletion, middle, and end) and then further compared at 24 and 48 h after the vesicles were made. $g(s^*)$ data sets obtained from separate preparations were normalized and graphically compared by fitting (Igor Pro version 3.1, Wavemetrics; Lake Oswego, OR) each data set to a Gaussian function and utilizing the centroid of each function to describe the *s* value for each preparation. The reduced data are presented as a single value with standard deviation and are derived from four data sets.

Electron microscopic analysis of the purified DOPC/DOPS vesicles was made to provide a visual assessment of the vesicle size range and homogenity and to confirm the absence of multilamellar structures. The vesicles were visualized using a negative staining protocol based on modification of the commonly used osmium tetroxide staining procedure (*43*). Vesicles were visualized at 20000× and 50000× magnification on a JEOL-T300 scanning electron microscope (housed in the Cell Imaging Facility, University of Vermont, College of Medicine).

Factor Va Activity Assessment in a Prothrombinase Assay. Factor Va cofactor activity was assessed in a microtiter plate DAPA assay (*47*). A sample containing factor Va (2 μL) was added (2 nM final concentration) to a mixture (total solution volume, 200 μL) containing prothrombin (1.4 μM), factor Xa (20 nM), PC_l/PS_l vesicles (20 μM), and DAPA (3.0 μM) in a black plastic 96 well microtiter plate (Dynex Technologies). Upon addition of factor Va with rapid mixing, the fluorescence emission intensity at 565 nm (280 nm excitation, high-pass KV550 emission filter) was monitored as a function of time. Fluorescence measurements were obtained using a FluoroMax-2 steady-state fluorometer equipped with a Micro-Max microtiter plate reader with fiber-optic coupling to the sample chamber (SPEX-ISA, Edison, NJ). Initial rate values were determined through linear regression analysis utilizing a software package, "Max-fit", written in our laboratory. The software "Max-fit" evaluates time-based fluorescence data using a reduced chi-squared error analysis over a moving window of data points to find a maximum slope. Data sets were acquired in duplicate from the fluorescence spectrophotometer and analyzed independently; the reduced cofactor vs activity plots were then compared and averaged to generate the data sets shown. In some cases, standard cuvette-based DAPA assays were performed in a T-format SLM-8000 fluorometer using the emission monochromator channel for sample signal collection; the data were analyzed identically with the omission of averaging (*48*).

Light Scattering Analysis: Determination of Δ *Molecular Mass.* A right angle light scattering analysis technique (*49*) was adapted to include kinetic analyses and the determination of molecular weight averages (M_w) of the factor Va product remaining on the vesicle surface during inactivation by APC. Factor Va binds the lipid membrane in part through a hydrophobic insertion sequence, and thus the K_d for membrane binding varies greatly upon altering the phospholipid headgroup spacing as is found in the different SUV and LUV populations (*49*). For this reason, it was imperative to demonstrate that the vesicles utilized in these experiments were SUV which were homogeneous by every method of analysis. The DOPC/DOPS vesicles used were characterized with respect to particle size and homogeneity (described above) to confirm that we were using small unilamellar vesicles (SUV) with no significant contamination of large unilamellar vesicles (LUV).

Upon addition of factor Va to the vesicles, the change in scattering intensity was utilized to calculate the ΔM_w of the starting vesicle·protein complex (*50*, *51*) using the formula (*49*):

$$\frac{I_2}{I_1} = \left[\frac{\left(\frac{\partial n}{\partial c}\right)_2}{\left(\frac{\partial n}{\partial c}\right)_1}\right]^2 \cdot \left[\frac{M_2}{M_1}\right]^2$$

$$\frac{M_1}{M_2} = \sqrt{\frac{I_1}{I_2}} \cdot \frac{\left(\frac{\partial n}{\partial c}\right)_2}{\left(\frac{\partial n}{\partial c}\right)_1} \qquad (1)$$

where I_1 = intensity due to vesicle alone, I_2 = intensity due to vesicle·protein complex, M_1 = calculated mass of vesicle alone (derived from ultracentrifugation), and the term $\partial n/\partial c$ represents the calculated refractive index gradient for the pure lipid or the vesicle·protein complex. The value for $\partial n/\partial c$ was calculated for each experiment based upon a weight fraction average according to the formula:

$$\left(\frac{[\text{Va}]}{[\text{Va}] + [\text{DOPC/DOPS}]}\right) \cdot \left(\frac{\partial n}{\partial c}\right)_{\text{Va}} + \left(\frac{[\text{DOPC/DOPS}]}{[\text{Va}] + [\text{DOPC/DOPS}]}\right) \cdot \left(\frac{\partial n}{\partial c}\right)_{\text{DOPC/DOPS}} = \left(\frac{\partial n}{\partial c}\right)_{\text{AVG}} \qquad (2)$$

where [Va] and [DOPC/DOPS] represent the weight concentration (g/mL) of each species and $(\partial n/\partial c)_{Va}$ and $(\partial n/\partial c)_{DOPC/DOPS}$ represent the refractive index gradient reference values for prothrombin and lipid vesicles, 0.192 and 0.172, respectively (*50*). The published value for prothrombin was used as a surrogate for factor Va in our calculations. In a typical experiment using 100 nM factor Va and 50 μM DOPC/DOPS, the calculated $\partial n/\partial c$ value is 0.186.

The M_1/M_2 ratio calculated from the light scattering data was utilized to define the average mass change observed per vesicle·protein complex. Fractional saturation terms describing vesicle occupancy (θ') and protein bound (θ) were derived using empirically defined binding parameters for factor Va and lipid vesicles. For each set of experimental

conditions, the number of factor Va bound per vesicle was calculated given a stoichiometry of 42 lipid headgroups occupied per factor Va molecule ($n = 42$), and a K_d of 2.7 nM (*10*). The maximum number of accessible phospholipids was calculated assuming that on average only 67% of the SUV phospholipid headgroups are surface-exposed to factor Va (*52*). The complete derivation is shown below:

$$\mathrm{Va{\cdot}L_S} \overset{K_d}{\longleftrightarrow} \mathrm{Va} + \mathrm{L_S}$$

$$K_d = \frac{([\mathrm{Va}]_t - [\mathrm{Va{\cdot}L_S}])*([\mathrm{L_S}]_t - [\mathrm{Va{\cdot}L_S}])}{[\mathrm{Va{\cdot}L_S}]}$$

$$\theta \equiv \frac{[\mathrm{Va{\cdot}L_S}]}{[\mathrm{Va}]_t}$$

$$\theta' \equiv \frac{[\mathrm{Va{\cdot}L_S}]}{[\mathrm{L_S}]_t}$$

expand K_d expression into quadratic form of θ or θ':

$$0 = (\theta)^2 - \left(1 + \frac{[\mathrm{L_S}]_t}{[\mathrm{Va}]_t} + \frac{K_d}{[\mathrm{Va}]_t}\right)(\theta) + \frac{[\mathrm{L_S}]_t}{[\mathrm{Va}]_t}$$

$$0 = (\theta')^2 - \left(1 + \frac{[\mathrm{Va}]_t}{[\mathrm{L_S}]_t} + \frac{K_d}{[\mathrm{L_S}]_t}\right)(\theta') + \frac{[\mathrm{Va}]_t}{[\mathrm{L_S}]_t}$$

number of sites per lipid $= i \therefore [\mathrm{L_s}] = [\mathrm{L_t}]*i = [\mathrm{L_t}]/n$

$$\theta = \frac{\left(1 + \frac{[\mathrm{L_t}]}{[\mathrm{Va}]_t*n} + \frac{K_d}{[\mathrm{Va}]_t}\right) - \sqrt{\left(1 + \frac{[\mathrm{L_t}]}{[\mathrm{Va}]_t*n} + \frac{K_d}{[\mathrm{Va}]_t}\right)^2 - (4)\left(\frac{[\mathrm{L_t}]}{[\mathrm{Va}]_t*n}\right)}}{2} \quad (3)$$

$$\theta' = \frac{\left(1 + \frac{[\mathrm{Va}]_t*n}{[\mathrm{L_t}]} + \frac{K_d*n}{[\mathrm{L}]_t}\right) - \sqrt{\left(1 + \frac{[\mathrm{Va}]_t*n}{[\mathrm{L}]_t} + \frac{K_d*n}{[\mathrm{L_t}]}\right)^2 - (4)\left(\frac{[\mathrm{Va}]_t*n}{[\mathrm{L}]_t}\right)}}{2}$$

From the fractional saturation of factor Va and lipid yielded by these formulas, the number of factor Va molecules bound per vesicle can be calculated and thus the molecular weight change (ΔM_w) associated with each protein species (from M_1/M_2).

Light Scattering: Experimental Determination of Factor Va Molecular Composition. All experiments were done in twice-filtered (0.45 μm pore size), degassed, dust-free HBS with 5 mM $CaCl_2$. The scattering signal observed for buffer alone was subtracted from all experimental observations to normalize the data to a zero value starting point. Then 100 nM factor Va (dialyzed and centrifuged to remove particulate matter) was preincubated with 50 μM DOPC/DOPS vesicles in a 4.0 mL quartz cuvette stirred gently with a micro stir bar. The scattering intensity signal was monitored with time to establish a stable initial value (2−3 min). Upon the addition of APC (0−75 nM), the scattering intensity signal was monitored continuously (0.5 s interval) for up to 30 min. Corrections for the initial scattering contribution due to the added APC binding the Va·lipid surface were made through successive additions of active site-inhibited APC (APC_I, 10−100 nM) to the vesicle complex with continuous monitoring of the scattering intensity. The absence of proteolytic activity in these APC_I preparations was demonstrated in the S-2236 chromogenic assay and through the presence of a stable light scattering signal for the Va·vesicle·APC_I complex obtained over 15 min of incubation at 100 nM APC_I (indicating no mass loss, i.e., no cleavage).

The data acquired utilizing active APC were evaluated according to the mass/scattering intensity relationship and the resulting molecular weight ratio, M_1/M_2 (eq 1), used to estimate the mass change for the vesicle·protein complex. Estimates of fractional saturation of factor Va and lipid were obtained from the quadratic solutions (eq 3), which were utilized to convert vesicle·protein mass change to an average mass change (ΔM_w) per factor Va molecule. This calculation was also utilized to assess lipid occupancy (always <20%), ensuring the availability of unoccupied lipid surface to bind APC. These derived mass loss data (from APC addition) as well as the raw intensity data were fit (Igor Pro version 3.1, Wavemetrics) to a single-exponential expression to evaluate the rate of mass change. The goodness of fit was evaluated through reduced chi-square error analysis, and residual plot distribution was examined in each case. The dependence of the mass loss, i.e., dissociation rate, on APC concentration was determined in a similar fashion from the calculated mass loss over time plots.

Mathematical Model of Factor Va Inactivation. The inactivation of factor Va by APC was modeled as a series of associations, dissociations, and cleavage reactions occurring on a membrane surface at saturating lipid concentrations. From the model, a system of first-order linear differential equations was constructed describing the rate of appearance and disappearance of each species assuming elementary kinetic behavior for each association, dissociation, and cleavage reaction. Initial values are established at time $t = 0$ by noting the concentration of factor Va, APC, and all other species. This system of equations is then an initial value problem which is intractable to explicit solution, but for which a series of solutions can be approximated. Using the Episode differential equation solver optimized for stiff equation systems and with the analytical Jacobian (The Scientist, version 2.01, MicroMath Inc., Salt Lake City, UT), a solution to this system of equations can be approximated quite rapidly and with relatively high precision and accuracy. This approach generates time-dependent concentration values for each species included in the computational model. The rate constants utilized, although derived from both the bovine and human systems, are assumed to describe globally the reaction kinetics for either human or bovine factor Va inactivation.

The model assumes a diffusion-limited second-order rate constant (k_1) for the associative encounter of Va and APC (assuming lipid-bound species). This rate constant (Va APC encounter) is assumed to be analogous to the rate constants for the rate-limiting independent lipid binding of factor Va and factor Xa measured for prothrombinase assembly, which provides an upper limit for the rapid two-dimensional diffusion encounter rate on the vesicle surface (*53*). Under conditions where APC is added to factor Va that is preequilibrated with the lipid, the rate of association is limited by the rate of diffusion of APC to the surface-bound factor

Va. The rate constant (k_2) for dissociation of the Va·APC Michaelis complex was deduced from the known K_d for the complex (7 nM = k_1/k_2) in correspondence to the published value (*53*). All possible LC species, A1A2·LC, A1·A2·LC, and A1·LC, were considered equivalent in their binding interactions with APC (defined by k_1, k_2 above). As modeled, the inactivation of factor Va is allowed to proceed with initial cleavage at either Arg^{306} or Arg^{505}. Initial cleavage at Arg^{662} was not modeled due to both kinetic considerations ($k_{662} \ll k_{505}$, k_{306}) and the observation that cleavage at this site alone (in the human system, Arg^{679}) does not appear to affect cofactor inactivation (*16*). As a starting point in our modeling, the second-order rate constants (k_{cat}/K_m) for cleavage at Arg^{306}, Arg^{505}, and Arg^{662} were taken from the literature and used to derive a first-order cleavage rate constant (k_3, k_5, k_6) (*16*, *17*, *20*) The first-order rate constants were approximated through assuming that the second-order rates were equivalent to k_{cat}/K_M and thus that the rate constant for each cleavage reaction (first order) (i.e., k_3, k_5, or k_6) could be initially approximated through the following manipulation: K_M* reported second-order rate = k_{cat}.

The first-order rate constant for the dissociation of cleaved factor Va was derived experimentally using light scattering analyses as described (k_7). In the formula notation used in this model, "Va_n" signifies a factor Va molecule cleaved at Arg^{505} (Va_5), Arg^{306} (Va_3), and Arg^{662} (Va_6). Thus, in the new notation, the model allows all factor Va species cleaved at Arg^{306} to dissociate (i.e., Va_3, $Va_{5\,3}$, $Va_{5\,3\,6}$, etc.) into the LC·A1 complex and the appropriate cleaved A2 domain fragments. The corollary collisional association second-order association rate constant (k_8) was estimated based on a lower limit K_d for the cleaved products of 10 μM (*27*) ($K_d = k_7/k_8$). The dissociation of intact factor Va (A1A2·LC) into A1A2 + LC was modeled using empirically defined rate constants for the forward (k_9) and reverse process (k_{10}) (*24*). The model does not directly account for surface binding competition between the reactants or products. However, all of the rate constants used were derived experimentally using lipid-mediated reactions or were estimated based upon presumed lipid-mediated rate processes. Thus, all reactions are modeled as occurring on a lipid surface (*30*). The binding constants for the LC and associated complexes with APC are all highly lipid-dependent, and the model utilizes only those measurements made on a lipid surface (*26*); thus this interaction should be robust in the model.

The fitness of the model was judged principally upon the correspondence between calculated inactivation profiles and experimental activity data derived from monitoring the of inactivation factor Va (200 nM) with APC (10 nM) using both DAPA and clotting assays. The calculation of theoretical cofactor activity is discussed below. The correspondence between experimental and theoretical cofactor activity plots was initially evaluated using either set of published cleavage rate constants. Manual iterations were then conducted through altering either the Arg^{506} (k_5) or the Arg^{306} (k_3) rate constants to values that produced good correlation between the model and experimental data. The rate constants thus derived are illustrated in Table 1 along with the published literature values.

Calculation of Theoretical Factor Va Activity. The inactivation of 200 nM factor Va by 5 nM APC was simulated using the model system. Theoretical cofactor activity measurements were generated according to the following formula which was derived to simulate the apparent cofactor activity expressed by factor Va in a prothrombinase assay using saturating factor Xa levels. The relative contributions of factor Va cleavage intermediates to the expressed activity were taken from published literature values (i.e., Va = 100% and Va_5 = 60%) (*1*, *18*). The first calculation assumes that bond cleavage mediates cofactor inactivation and utilizes activity approximations for intermediate species that correspond to their activities as assessed in a DAPA assay:

Table 1: Rate Constants Utilized in the Kinetic Model[a]

rate constant	model rate (s^{-1})	model rate ($M^{-1}\,s^{-1}$)	reference value	derived rate ($M^{-1}\,s^{-1}$)
k_1		1.0×10^8	$1.0 \times 10^8\,M^{-1}\,s^{-1}$ [b]	
k_2	0.7		$0.7\,s^{-1}$ [c]	
k_3	0.064		$(1.7-2.5) \times 10^6\,s^{-1}$ [d]	9.1×10^6
k_5	1.00		$(3.0-4.3) \times 10^7\,s^{-1}$ [d]	1.42×10^8
k_6	5.2×10^{-4}		$5.2 \times 10^{-4}\,s^{-1}$ [e]	
k_7	0.028			
k_8		2.57×10^3	$2.57 \times 10^3\,M^{-1}\,s^{-1}$ [f]	
k_9	1.72×10^{-5}		$1.72 \times 10^{-5}\,s^{-1}$ [g]	
k_{10}		2.63×10^3	$2.63 \times 10^3\,M^{-1}\,s^{-1}$ [g]	

[a] Rate constants listed were either taken from literature values (*b*−*d*) or established by comparative iteration of the model based upon visual inspection of the predicted progress curves and experimental data. Columns labeled "model rate" contain the rate constant values utilized in the modeling experiments. The published values are shown as reference values in the fourth (reference value) column. The fifth column (derived rate) illustrates the pseudo-second-order rate constant, based upon the modeled first-order process, for cleavage at each site. These values were mathematically derived using the defining relationship k_{cat}/K_m where K_m was approximated as k_2/k_1 and k_{cat} was taken as either k_3 or k_5. Reference value citations: [b](*53*); [c](*24*). [d] Range stated encompasses two independent determinations (*16*, *17*). [e](*17*); [f](*53*); [g](*24*).

% app act. cleavage-dependent inactivation

$$\equiv \left[\frac{([Va]_{free} + [Va{\cdot}APC])}{[Va]_{total}}\right]*100 + \left[\frac{([Va_5]_{free} + [Va{\cdot}APC])}{[Va]_{total}}\right]*60 \quad (4)$$

In this calculation, cleavage at Arg^{306} is assumed to inactivate the cofactor. A simplified version of this (leaving out the second term) is utilized to calculate the apparent cofactor activity that would be apparent in a clotting assay, where cleavage at Arg^{506} inactivates the cofactor. A second method of cofactor activity calculation is shown below in which the inactivation of the cofactor is assumed to occur as a consequence of dissociation of the cleaved products; thus, the cleaved associated products are assumed to retain their respective cofactor activities. The relative cofactor activity of the Arg^{306}-cleaved associated products is unknown and was assumed to be equivalent to the Arg^{505} product, although this must be considered an upper limit. These two methods of cofactor activity calculation were utilized to generate theoretical activity plots:

% apparent activity dissociation-dependent inactivation

$$\equiv \left[\frac{([Va]_{free} + [Va{\cdot}APC])}{[Va]_{total}}\right]*100 + \left[\frac{[Va_5]_{free} + [Va_5{\cdot}APC] + [Va_3]_{free} + [Va_3{\cdot}APC] + [Va_{5\,3}]_{free} + [Va_{3\,5}{\cdot}APC] + [Va_{3\,5\,6}]_{free} + [Va_{3\,5\,6}{\cdot}APC]}{[Va]_{total}}\right]*60 \quad (5)$$

Calculation of Theoretical Factor Va^{LEIDEN} Inactivation Profiles. The inactivation of factor Va^{LEIDEN} was simulated by eliminating the Arg^{506} cleavage site within the model ($k_5 = 0.0$ s^{-1}). The inactivation of 200 nM factor Va^{LEIDEN} with 10 nM APC was then simulated, and the predicted activity profiles were calculated as described previously. These activity predictions were then evaluated by comparison with the inactivation of normal factor Va and by comparison to the literature observations regarding the observed magnitude of the inactivation resistance profile as a function of the cofactor activity assay conditions, i.e., DAPA vs clotting assay.

Evaluation of the Inhibitory Potential of the LC and Associated Products. 200 nM bovine factor Va was treated with 5 nM APC and the cofactor activity monitored over time using the DAPA assay. Upon complete inactivation of factor Va, an additional bolus of factor Va (200 nM) was added to the reaction mixture and the cofactor activity monitored over time. The concentration of APC active sites was monitored throughout the experiment using a peptidyl-fluorogenic substrate (D-VPR-ANSNHC$_4$H$_9$) assay as described previously (*12*, *18*). These successive addition experiments evaluate the expressed APC activity toward macromolecular substrates (intact factor Va) in the presence of reaction products such as the A1·LC complex. An additional analysis utilizing purified reaction components was accomplished using purified bovine LC preparations. In these experiments, 100 μM PC/PS was utilized, and 40 nM bovine factor Va was treated with 2 nM APC in the presence or absence of purified LC of either the M_r 72 000 or the M_r 74 000 species at varying concentrations, 400 nM, 100 nM, 40 nM, and 4 nM. Factor Va and LC were preincubated with PC/PS at 37 °C for 5 min prior to the addition of APC. Upon addition of APC, the cofactor activity was monitored over time and compared to the profile obtained in the absence of exogenously added free LC. The relative cofactor activity of factor Va was determined using the DAPA assay.

Theoretical Evaluation of the Inhibitory Potential of the LC-Associated Products in the Inactivation of Factor Va. The correlation between the experimental data demonstrating product inhibition, using either successive substrate addition or addition of free LC, and the modeled inhibition mechanism was evaluated through seeding the model with either free LC or LC·A1 at 200 nM and evaluating the inactivation of factor Va (200 nM) with APC (10 nM).

RESULTS

Determination of the Mass of Factor Va·(DOPC/DOPS) Vesicles. DOPC/DOPS vesicles exhibited a single $g(s^*)$ peak corresponding to an observed S of 3.2 ± 0.2 S (four preperations) (Table 3) (*46*). Whole boundary fitting (using the software "Svedberg") to s/D (MW) yielded a molecular weight estimate of $(2.0 \times 10^6) \pm (1.0 \times 10^5)$, corresponding to the range found from five different vesicle preparations and in agreement with similar measurements (Table 3) (*43*, *52*). Scanning electron microscopic analyses confirmed these results and demonstrated a SUV population with a narrow size range and no apparent contamination by either LUV or multilamellar vesicles. Upon addition of the vesicles to the cuvette containing buffer, the corresponding light scattering intensity, I_1, was 318 000 cps. Upon addition of factor Va, the resulting intensity, I_2, was 970 000 cps. The molecular weight change per vesicle upon addition of factor Va was calculated from eq 1 as 946 000 using a $(dn/dc)_1$ value of 0.172 (lipid) and a corrected (weight average) $(dn/dc)_2$ value of 0.186 for the protein·vesicle complex (eq 2). The total change in protein·vesicle molecular weight was used to determine the expected mass change for each factor Va bound using the quadratic solutions derived for protein and lipid saturation. At 50 μM DOPC/DOPS and 100 nM bovine factor Va ($K_d = 2.7$ nM, $n = 42$), eq 3 predicts that >99% of the protein is bound to the surface while 12.5% of the total exposed lipid surface is occupied, with an average of 5.05 factor Va molecules bound per vesicle. Thus, the calculated average molecular weight change per Va on the vesicle surface is M_r 187 000 (±13 000), in reasonable agreement with the expected value of M_r 170 000. The addition of EDTA (10 mM) to the protein·vesicle complex releases the HC of factor Va, leaving the LC bound to the membrane (*26*). The calculated molecular weight change due to release of the HC upon EDTA addition, M_r 105 000 ± 5000, is in reasonable agreement to the expected loss of M_r 94 000 for the bovine HC (Table 3).

Determination of Mass Loss Due to Factor Va Fragment Dissociation upon Cleavage by APC. The molecular weight change per factor Va bound was calculated as detailed above for the addition of 100 nM bovine factor Va to 50 μM DOPC/DOPS. Upon addition of APC at either 0, 10, 20, 50, or 75 nM, the light scattering intensity was followed at 0.5 s intervals until a stable value was obtained (5−15 min). Figure 1A shows the uncorrected intensity traces. Upon addition of 10 nM APC (+), the scattering intensity decreased from 1.0×10^6 cps to a final value of 830 000 cps within 720 s. The few scattered data points contained in each data set are due to the sensitivity of this technique to solution contamination by dust particles. However, the low level of noise generally observed in these data allows the molecular weight changes to be calculated with confidence. This low level of noise can only be attained with careful filtration and the use of highly selected vesicle populations. The addition of 20 nM APC (×) is accompanied by a reduction in scattered intensity from an initial value of 1.0×10^6 cps to a plateau of 830 000 cps within 360 s. The data sets obtained upon addition of both 50 and 75 nM APC are nearly identical to each other (○, △), starting at 1.0×10^6 cps and reaching stable plateau values of 830 000 cps at 210 and 180 s, respectively. From these data, the corresponding traces of the time-dependent molecular weight loss from the vesicle surface were generated as described under Methods (Figure 1B). The displayed data (Figure 1B) were calculated using base line corrected intensity values and assuming a $(dn/dc)_1/(dn/dc)_2$ ratio of 1.0. Inspection of Figure 1B reveals that treatment of factor Va at each APC concentration shown leads to a limiting mass loss of 54 000 daltons per factor Va molecule exhibiting the same kinetics as detailed for the raw intensity data (Figure 1B). The observed mass loss of 54 000 daltons/molecule corresponds to the mass loss expected for dissociation of the cleaved A2 fragments, $A2_N \cdot A2_C + A2_{C-peptide}$ (53 000 daltons), from the remainder of the molecule (*27*).

Table 2: Differential Equations Derived from Figure 6[a]

$$\frac{d[Va]}{dt} = [Va{\cdot}APC]{*}k_2 - [Va][APC]{*}k_1 + [HC][LC]{*}k_{10} - [Va]{*}k_9 \quad (6)$$

$$\frac{d[Va{\cdot}APC]}{dt} = [Va][APC]{*}k_1 - [Va{\cdot}APC]{*}(k_2 + k_3 + k_5) \quad (7)$$

$$\frac{d[HC]}{dt} = [Va]{*}k_9 - [HC][LC]{*}k_{10} \quad (8)$$

$$\frac{d[Va_5]}{dt} = [Va_5{\cdot}APC]{*}k_2 + [HC_5][LC]{*}k_{10} - [Va_5][APC]{*}k_1 - [Va_5]{*}k_9 \quad (9)$$

$$\frac{d[Va_5{\cdot}APC]}{dt} = [Va_5][APC]{*}k_1 + [Va{\cdot}APC]{*}k_5 - [Va_5{\cdot}APC]{*}(k_2 + k_3 + k_6) \quad (10)$$

$$\frac{d[HC_5]}{dt} = [Va_5]{*}k_9 - [HC_5][LC]{*}k_{10} \quad (11)$$

$$\frac{d[Va_3]}{dt} = [Va_3{\cdot}APC]{*}k_2 + [HC_3][LC]{*}k_{10} + [Va_{LC{\cdot}A1}][Va_{A3}]{*}k_8 - [Va_3][APC]{*}k_1 - [Va_3]{*}(k_7 + k_9) \quad (12)$$

$$\frac{d[Va_3{\cdot}APC]}{dt} = [Va{\cdot}APC]{*}k_3 + [Va_3][APC]{*}k_1 + [Va_{LC{\cdot}A1}{\cdot}APC][Va_{A3}]{*}k_8 - [Va_3{\cdot}APC]{*}(k_2 + k_5 + k_6 + k_7) \quad (13)$$

$$\frac{d[HC_3]}{dt} = [Va_3]{*}k_9 - [HC_3][LC]{*}k_{10} \quad (14)$$

$$\frac{d[Va_{53}]}{dt} = [Va_{53}{\cdot}APC]{*}k_2 + [HC_{53}][LC]{*}k_{10} + [Va_{LC{\cdot}A1}][Va_{A53}]{*}k_8 - [Va_{53}][APC]{*}k_1 - [Va_{53}]{*}(k_7 + k_9) \quad (15)$$

$$\frac{d[Va_{53}{\cdot}APC]}{dt} = [Va_5{\cdot}APC]{*}k_3 + [Va_3{\cdot}APC]{*}k_5 + [Va_{53}][APC]{*}k_1 + [Va_{LC{\cdot}A1}{\cdot}APC][Va_{A53}]{*}k_8 - [Va_{53}{\cdot}APC]{*}(k_2 + k_6 + k_7) \quad (16)$$

$$\frac{d[HC_{53}]}{dt} = [Va_{53}]{*}k_9 - [HC_{53}][LC]{*}k_{10} \quad (17)$$

$$\frac{d[Va_{36}]}{dt} = [Va_{36}{\cdot}APC]{*}k_2 + [HC_{36}][LC]{*}k_{10} + [Va_{LC{\cdot}A1}][Va_{A36}]{*}k_8 - [Va_{36}][APC]{*}k_1 - [Va_{36}]{*}(k_7 + k_9) \quad (18)$$

$$\frac{d[Va_{36}{\cdot}APC]}{dt} = [Va_3][APC]{*}k_1 + [Va_3{\cdot}APC]{*}k_6 + [Va_{LC{\cdot}A1}{\cdot}APC][Va_{A36}]{*}k_8 - [Va_{36}{\cdot}APC]{*}(k_2 + k_5 + k_7) \quad (19)$$

$$\frac{d[HC_{36}]}{dt} = [Va_{36}]{*}k_9 - [HC_{36}][LC]{*}k_{10} \quad (20)$$

$$\frac{d[Va_{56}]}{dt} = [Va_{56}{\cdot}APC]{*}k_2 + [HC_{56}][LC]{*}k_{10} + [Va_{56}][APC]{*}k_1 - [Va_{56}]{*}k_9 \quad (21)$$

$$\frac{d[Va_{56}{\cdot}APC]}{dt} = [Va_5{\cdot}APC]{*}k_6 + [Va_{56}][APC]{*}k_1 - [Va_{56}{\cdot}APC]{*}(k_2 + k_3) \quad (22)$$

$$\frac{d[HC_{56}]}{dt} = [Va_{56}]{*}k_9 - [HC_{56}][LC]{*}k_{10} \quad (23)$$

$$\frac{d[Va_{536}]}{dt} = [Va_{536}{\cdot}APC]{*}k_2 + [HC_{536}][LC]{*}k_{10} + [Va_{LC{\cdot}A1}][Va_{A536}]{*}k_8 - [Va_{536}]{*}(k_7 + k_9) - [Va_{536}][APC]{*}k_1 \quad (24)$$

$$\frac{d[Va_{536}{\cdot}APC]}{dt} = [Va_{53}{\cdot}APC]{*}k_6 + [Va_{36}{\cdot}APC]{*}k_5 + [Va_{56}{\cdot}APC]{*}k_3 + [Va_{536}][APC]{*}k_1 + [Va_{LC{\cdot}A1}{\cdot}APC][Va_{A356}]{*}k_8 - [Va_{536}{\cdot}APC]{*}(k_2 + k_7) \quad (25)$$

$$\frac{d[HC_{536}]}{dt} = [Va_{536}]{*}k_9 - [HC_{536}][LC]{*}k_{10} \quad (26)$$

$$\frac{d[Va_{LC{\cdot}A1}]}{dt} = [Va_3 + Va_{36} + Va_{35} + Va_{356}]{*}k_7 - [Va_{LC{\cdot}A1}]([Va_{A3}] + [Va_{A35}] + [Va_{A36}] + [Va_{A356}]){*}k_8 - [Va_{LC{\cdot}A1}][APC]{*}k_1 + [Va_{LC{\cdot}A1}{\cdot}APC]{*}k_2 \quad (27)$$

$$\frac{d[Va_{LC{\cdot}A1}{\cdot}APC]}{dt} = ([Va_3{\cdot}APC] + [Va_{36}{\cdot}APC] + [Va_{53}{\cdot}APC] + [Va_{536}{\cdot}APC]){*}k_7 + [Va_{LC{\cdot}A1}][APC]{\cdot}k_1 - [Va_{LC{\cdot}A1}{\cdot}APC]{*}k_2 - ([Va_{A3}] + [Va_{A35}] + [Va_{A36}] + [Va_{A356}]){*}k_8[Va_{LC{\cdot}A1}{\cdot}APC] \quad (28)$$

Table 2 (Continued)

$$\frac{dLC}{dt} = ([Va] + [Va_5] + [Va_3] + [Va_{56}] + [Va_{35}] + [Va_{36}] + [Va_{536}])^*k_9 - ([HC] + [HC_5] + [HC_3] + [HC_{53}] + [HC_{36}] + [HC_{56}] + [HC_{536}])^*[LC]^*k_{10} - [LC][APC]^*k_1 + [LC\cdot APC]^*k_2 \quad (29)$$

$$\frac{dLC\cdot APC}{dt} = [LC][APC]^*k_1 - [LC\cdot APC]^*k_2 \quad (30)$$

$$\frac{dVa_{A3}}{dt} = ([Va_3] + [Va_3\cdot APC])^*k_7 - [Va_{LC\cdot A1}\cdot APC][Va_{A3}]^*k_8 - [Va_{LC\cdot A1}][Va_{A3}]^*k_8 \quad (31)$$

$$\frac{dVa_{A53}}{dt} = ([Va_{5\,3}] + [Va_{5\,3}\cdot APC])^*k_7 - [Va_{LC\cdot A1}\cdot APC][Va_{A53}]^*k_8 - [Va_{LC\cdot A1}][Va_{A53}]^*k_8 \quad (32)$$

$$\frac{dVa_{A36}}{dt} = ([Va_{3\,6}] + [Va_{3\,6}\cdot APC])^*k_7 - [Va_{LC\cdot A1}\cdot APC][Va_{36}]^*k_8 - [Va_{LC\cdot A1}][Va_{A36}]^*k_8 \quad (33)$$

$$\frac{dVa_{A536}}{dt} = ([Va_{5\,3\,6}] + [Va_{5\,3\,6}\cdot APC])^*k_7 - [Va_{LC\cdot A1}\cdot APC][Va_{A536}]^*k_8 - [Va_{LC\cdot A1}][Va_{A536}]^*k_8 \quad (34)$$

$$\frac{dAPC}{dt} = ([Va\cdot APC] + [Va_5\cdot APC] + [Va_3\cdot APC] + [Va_{5\,3}\cdot APC] + [Va_{3\,6}\cdot APC] + [Va_{5\,6}\cdot APC] + [Va_{5\,3\,6}\cdot APC] + [LC\cdot APC] + [Va_{LC\cdot A1}\cdot APC])^*k_2 - ([Va] + [Va_5] + [Va_3] + [Va_{5\,3}] + [Va_{5\,6}] + [Va_{3\,6}] + [Va_{5\,3\,6}] + [Va_{LC}] + [Va_{LC\cdot A1}])^*[APC]^*k_1 \quad (35)$$

[a] The equations are numbered sequentially starting in the text; thus, eq 5 represents the first of 29 (5−34) equations used to generate the computational model for factor Va inactivation. The text details the derivation, and Figure 6 illustrates the reaction diagram which these equations describe. Equations 7, 10, 13, 16, 19, 22, and 25 are utilized to describe the HC−LC association/dissociation equilibrium between associated factor Va species; these equilibria are not shown in the reaction diagram (Figure 6). In addition, eqs 11, 12, 14, 15, 17, 18, 20, 21, 23, 24, and 26, 27 all involve terms detailing the dissociation/association equilibrium between cleaved associated and cleaved dissociated factor Va species. In Figure 6, these species are grouped as HCF.

Table 3: Solution Parameters for DOPC/DOPS Vesicles and Their Protein Complexes Utilized in This Research[a]

species	$g(s^*)$[b]	calculated M_r[c]	expected[d]
vesicles	3.2 ± 0.2	$(2.0 \times 10^6) \pm (1.0 \times 10^5)$[e]	−
Va·vesicle	−	2.94×10^6	2.84×10^6
Va	−	1.87×10^5 [f]	1.69×10^5
LC	−	8.2×10^4 [g]	7.4×10^4
HC	−	1.05×10^5 [g]	9.5×10^4
Va_I·vesicle	−	2.67×10^6	2.58×10^6
Va_I Soln	−	5.4×10^4	5.3×10^4
Va_I	−	1.15×10^5	1.16×10^5

[a] Mass estimates for the species listed were derived based upon the light scattering equation and rely additionally upon estimates of the stoichiometry of binding. [b] Results are presented (±standard deviation) for duplicate analyses of sedimentation velocity experiments on DOPC/DOPS using the $g(s^*)$ analyses (4 preparations). [c] The calculated M_r for each species (aggregate weight for complex species) derived from the light scattering equation using primary data as discussed under Methods. [d] The (published values) accepted molecular weight of each species, to be used in comparison to the derived light scattering data. [e] From analysis of sedimentation data as in Methods. [f] This value is determined by calculating the occupancy of each vesicle (number of protein bound) followed by simple math to calculate the mass per particle bound. [g] Addition of EDTA to the vesicle/protein complex leads to dissociation of the HC; thus, calculation of the remaining particle mass and derivation (as in *f*) of the mass bound allow determination of the mass of both the HC (solution) and LC (vesicle bound).

Determination of the Kinetics of Factor Va Dissociation upon APC Cleavage. Each of the curves shown in Figure 1 were utilized to derive the rates for the dissociation process as a function of APC concentration. The raw intensity data were corrected for a small scattering increase found upon addition of APC to the vesicle surface in the absence of factor Va. This correction for the measured scattering intensity increase was confirmed by APC_I addition (10, 20, 50, and 75 nM) to Va·DOPC/DOPS vesicles, yielding four corrected data sets for subsequent curve fitting (the maximum correction was 35 000 cps, at 75 nM APC_I). Without these corrections, a slight increase (the absolute value of which is dependent upon the APC concentration used) in the intensity data is found in each case immediately following APC addition which complicates fitting to a single-exponential expression. Figure 2A shows a representative single-exponential fit and residual plot obtained from the corrected curves in Figure 1A at 75 nM APC, where a rate of 0.028 s^{-1} was found. Figure 2B shows an independent fit and residual plot obtained using the derived mass change per factor Va vs time (Figure 1B, 75nM APC); a rate identical to that in Figure 2A was calculated. Similar treatments were performed on each of the other data sets shown in Figure 1A,B and the derived rate data plotted as a function of APC concentration (Figure 3). All of the data are adequately fit by a single-exponential function, and higher order fitting (e.g., double exponential) offered no improvement. Initially the dissociation rate increases linearly with increasing APC concentration; however, at concentrations greater than 20 nM APC, the rate begins to plateau and reaches a final value of 0.028 s^{-1} at APC concentrations above 50 nM. The data obtained reasonably define a limiting rate that is independent of APC concentration. This value represents the unimolecular dissociation rate constant (0.028 s^{-1}) for the loss of the cleaved A2 domain, $A2_N\cdot A2_C + A2_{C-peptide}$, liberated from the vesicle surface by cleavage at Arg^{306} (*27*). No other process appears to contribute to the mass loss described by the light scattering profiles.

Comparison between the Observed Light Scattering Signal and Factor Va Cofactor Activity. The raw scattering data obtained upon addition of 10, 20, 50, and 75 nM APC were normalized to a scale between 100 and 0. In a separate set of experiments, the inactivation of 100 nM bovine factor Va on 50 μM PC_l/PS_l vesicles following treatment with 10,

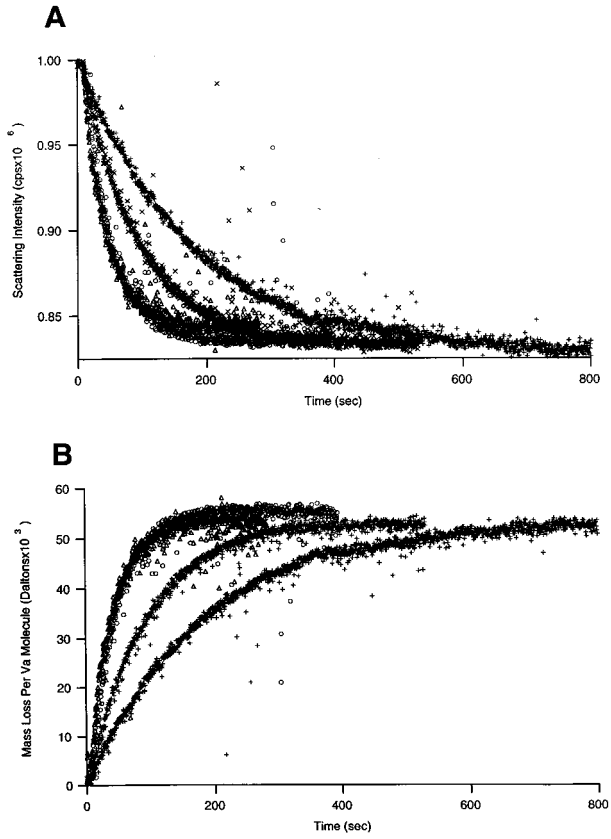

FIGURE 1: Light scattering analysis of factor Va inactivation. The inactivation of 100 nM bovine factor Va on 50 μM DOPC/DOPS was analyzed using 10, 20, 50, and 75 nM APC. After equilibration of factor Va on DOPC/DOPS vesicles, APC was added and the light scattering signal was monitored at 0.5 s intervals. (A) Upon addition of 10 nM APC (+), the scattering intensity signal decreased by 17% in amplitude over a 15 min period. Upon addition of 20 nM APC (×), the scattering intensity signal decreased by 17% in amplitude over a 7 min period. Upon addition of 50 nM (○) and 75 nM (△) APC, the light scattering intensity signal decreased by 17% in amplitude over a 3.5 min time course. (B) This panel displays the time-dependent derived mass loss from the DOPC/DOPS vesicle surface; the data in panel A were utilized to derive panel B according to the calculations outlined under Methods. Upon addition of 10 nM APC (+), a total mass of M_r 54 000 was lost from the vesicle surface over a 15 min period. Upon addition of 20 nM APC (×), a total mass of M_r 54 000 was lost from the vesicle surface over a 7 min period. Upon addition of 50 nM (○) and 75 nM (△) APC, a total mass of M_r 54 000 was lost from the vesicle surface over a 3.5 min time course.

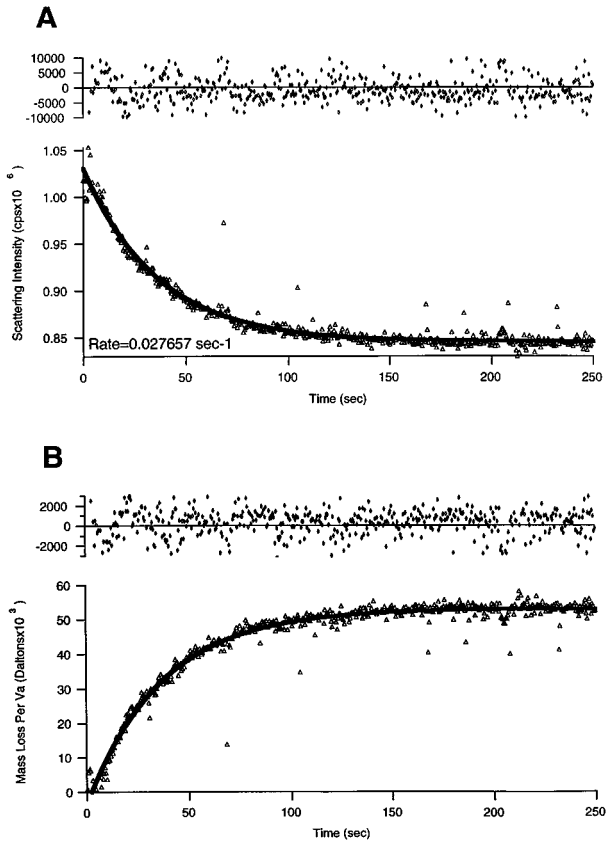

FIGURE 2: Analysis of the rate of factor Va dissociation upon APC cleavage. The raw scattering intensity signal and derived mass change shown in Figure 1 were fit to a single-exponential expression to determine the rate of change. (A) This panel illustrates the goodness of fit obtained upon fitting the raw intensity signal obtained upon addition of 75 nM (△) APC (Figure 1, panel A). The raw data are shown as (△); the derived fit is illustrated as a thick solid line. The upper axis illustrates the residual plot (data-fitted function) (◇) and shows random deviations from the zero line. The slight negative bias is due to the inherent noise present in the raw data which is always positive due to dust particle scattering and slightly influences the fit due to the use of a nonlinear least-squares fitting algorithm. The fitted rate constant describing the illustrated function is displayed in the lower left corner. (B) This panel illustrates the goodness of fit obtained upon fitting the derived mass loss signal obtained upon the addition of 75 nM (△) APC (Figure 1, panel B). The mass loss is shown as (△); the derived fit is illustrated as a thick solid line. The upper axis illustrates the residual plot (◇) and shows random deviations from the zero line. The slight positive bias is due to the inherent noise in the raw data which when transformed to mass results in an apparent larger mass loss signal; as a result of the fitting algorithm (see above), this weights the fit to a slightly lower value. The same rate constant as obtained in panel A was found.

20, 50, or 75 nM APC was monitored using the DAPA assay (10 nM factor Xa). The initial rate of prothrombin activation obtained at each time point during the inactivation reaction was calculated and normalized to a percent activity scale. Figure 4 shows a comparison between the normalized activity and light scattering intensities obtained at each APC concentration over the initial 100 s of inactivation; the symbols are as follows: 75 nM APC (△), 20 nM APC (×), and 10 nM APC (+). It can be seen that under all APC concentrations utilized the observed cofactor inactivation and the light scattering signal are similar. Due to the rather large time interval required for the measurement of activity, it is difficult to more closely space data points; however, the two measurements yield equivalent results over a large APC concentration and activity range (10−75 nM APC, 100−20% activity).

Determination of the Inhibitory Effect of the Factor Va LC and LC Complexes. Previous observations regarding the binding of the free LC and associated complexes to APC suggested that the evolution of cleaved dissociated LC products (principally, LC·A1) would generate a competing pool of APC binding sites. To evaluate the inhibitory potential of these LC complexes, the inactivation of 200 nM bovine factor Va on 50 μM PC_l/PS_l using 5 nM APC was monitored in a DAPA assay. Figure 5 shows the cofactor activity (○) obtained following addition of APC. After 30 min incubation, the cofactor activity obtained was <5%, and a second addition of factor Va (200 nM) was made from a concentrated stock (<2% volume change) and a second

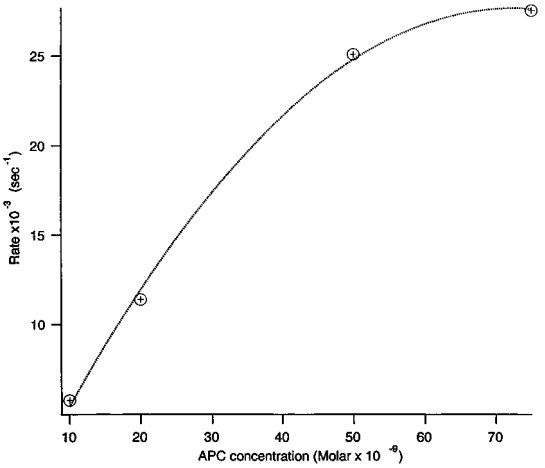

FIGURE 3: Dissociation rate constant dependence upon APC concentration. The results obtained from fitting all data sets shown in Figure 1B are shown plotted vs the concentration of APC used in the experiment. The hyperbolic plot illustrates a saturation in rate above 50 nM APC and describes the rate-limiting unimolecular dissociation rate constant as 0.028 s^{-1}.

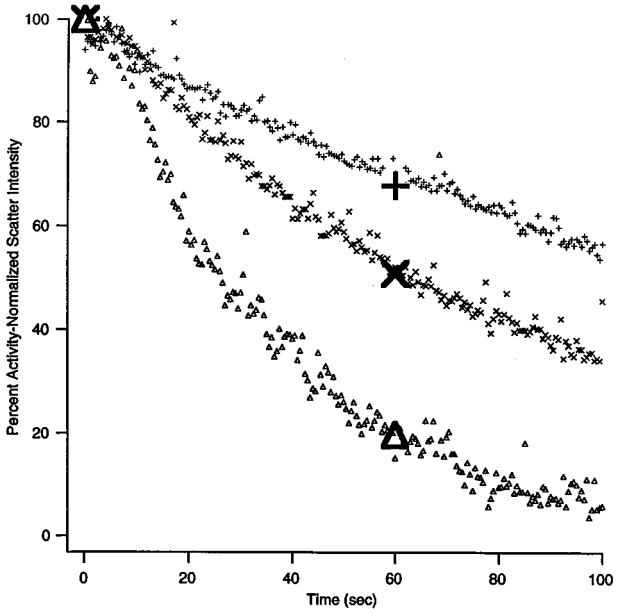

FIGURE 4: Comparison between the raw light scattering signal and the cofactor activity during APC inactivation of factor Va. The linkage between factor Va inactivation and dissociation was examined through a direct comparison of the light scattering trace and simultaneous cofactor activity assessment of factor Va in a DAPA assay. The light scattering data obtained upon addition of 10, 20, and 75 nM APC were normalized to a scale between 100 and 0 (simple arithmetic). These data were then plotted along with the cofactor activity data obtained in a DAPA assay (normalized to percent activity) to allow a direct comparison between the dissociation state (reflected in the light scattering trace and the cofactor activity). The cofactor activity at 0 and 1 min is plotted as 10 nM APC (+), 20 nM APC (×), and 75 nM APC (△). The normalized light scattering traces are illustrated using the symbols as shown in Figures 1 and 2.

decay curve for cofactor activity generated (●). The concentration of APC active sites was monitored using a peptidyl-fluorescent substrate, D-VPR-ANSNHC$_4$H$_9$, allowing picomolar APC detection (*18*); these measurements showed no loss of APC activity during the time course of the experiments, indicating a constant level of APC activity. At 4 min, 27% of the cofactor activity remained after the addition of APC. In contrast, upon a second addition of

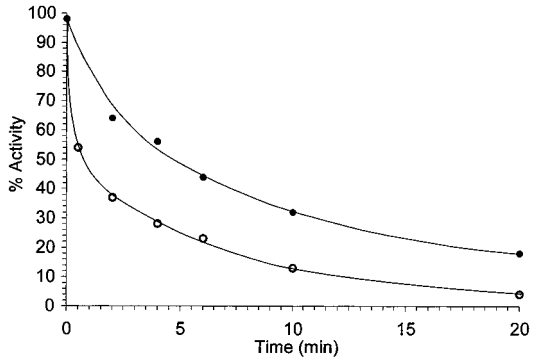

FIGURE 5: Analysis of the inhibitory potential of the factor Va LC and its associated complexes. The inactivation of 200 nM bovine factor Va on 100 μM PC/PS using 10 nM APC was monitored using the DAPA assay with 10 nM factor Xa. The open circles (○) are representative of the cofactor activity obtained upon addition of APC to the described reaction mixture and measured at 1, 2, 4, 6, 10, and 20 min. After 30 min of incubation, when the measured cofactor activity was less than 2% a second addition of factor Va (200 nM) was made and the cofactor activity analyzed immediately and at the time points indicated. The measured cofactor activity is shown as the solid circles (●).

substrate (Va), 56% of the activity remained at the 4 min time point (a 24% difference). Similarly, at 10 min, 10% activity remained after the addition of APC whereas 34% remained after the second addition of substrate (a 24% difference). The significant difference between the two cofactor activity plots is due to the sequestering of APC into nonproductive LC complexes (product inhibition) arising as a consequence of $A2_N{\cdot}A2_C + A2_{C-peptide}$ dissociation, thus generating

A1·LC complexes. This was confirmed in experiments using both purified light chain species (M_r 72 000 and 74 000). Mixtures of 40 nM bovine factor Va, 100 μM PC/PS, and varying concentrations of either LC component (0, 10, 50, 200, 400 nM) were incubated with 2 nM APC, and the cofactor activity was monitored over time. In these experiments, a similar level of inhibition was observed at all LC concentrations over 10 nM, in correspondence to the reported K_d for the LC APC interaction of 7 nM (*26*) (data not shown). Both LC components were equally active in their inhibitory potential toward APC, suggesting no difference in their affinity for or ability to bind APC.

A Quantitative Description of Factor Va Inactivation by APC. The reaction diagram shown in Figure 6 illustrates the basic scheme for the inactivation of factor Va by APC. The model consists of a series of linear first-order differential equations derived from inspection of Figure 6. As an example illustrating the derivation of the equations (Table 1) from the reaction diagram (Figure 6), consider the relationship describing the factor Va·APC concentration time dependence during a reaction. The following processes are modeled:

$$\text{Va} + \text{APC} \xrightarrow{k_1} \text{Va}{\cdot}\text{APC}$$

$$\text{Va}{\cdot}\text{APC} \xrightarrow{k_2} \text{Va} + \text{APC}$$

$$\frac{d[\text{Va}]}{dt} = [\text{Va}{\cdot}\text{APC}]^*k_2 - [\text{Va}]^*[\text{APC}]^*k_1$$

This expression (eq 6, Table 2) is in turn related to the expression for the concentration of Va·APC that includes the rate process for cleavage at Arg^{505} or Arg^{306} (eq 7, Table

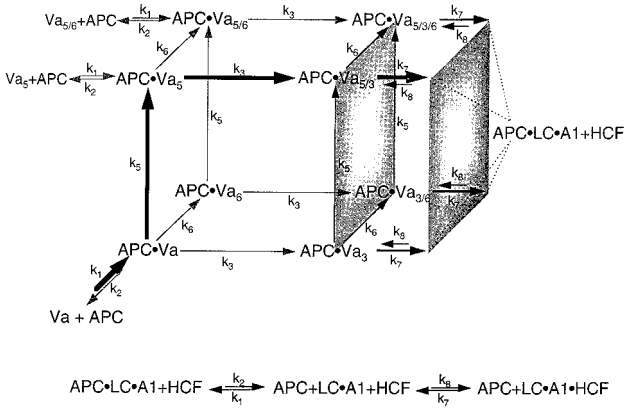

FIGURE 6: Factor Va inactivation: reaction diagram. The inactivation of factor Va was modeled according to a random cleavage process. Starting in the lower left corner, once APC binds factor Va three possible cleavage sites are possible. In the computer model, initial cleavage at Arg^{662} is ignored due to the large difference in rate compared to cleavage at $Arg^{306,505}$; this pathway is, however, illustrated for completeness. The cleaved APC Michaelis product complexes are allowed to dissociate into free APC and the product according to the equilibrium dictated by k_1,k_2. Subsequent cleavage events at the remaining sites, i.e., cleavage at Arg^{306} in the Va_5 (cleaved at Arg^{505}) product, occur according to their unique rate constants; given infinite time and no dissociation, the reaction will end up in the upper right corner, yielding totally cleaved Va. The shaded right face of the cube contains all possible Va species that have been cleaved at Arg^{306}; each of these products may independently undergo dissociation of the A2 domain fragments at rate k_7. For simplicity, the dissociated products have been grouped as APC·LC·A1 + HCF (heavy chain fragments). Once dissociated, the cleaved APC product complex may dissociate according to the equilibrium k_1,k_2. The dissociated LC·A1 + HCF products are in an equilibrium with the associated product according to k_7, k_8. In all cases, all associated HC·LC species whether cleaved or intact are in an equilibrium with the free LC and associated HC species. This equilibrium has been intentionally left off the diagram for simplicity since it affects all species on the cube; it is, however, defined by k_9, k_{10} (Table 2).

2). Most of the equations shown in Table 1 are illustrated in Figure 6; omitted are those equations describing the dissociation of all factor Va species, e.g., A1A2·LC into LC+A1A2, which are described by a simple K_d expression defined by k_9 and k_{10}, the experimentally determined forward and reverse rate constants (*24*) (eqs 6, 8, 9, 11, 12, 14, 15, 17, 18, 20, 21, 23, 24, 26, 29 of Table 2). The rate constants utilized to solve the differential equations are shown in Table 3 as well as two independent sets of experimentally determined second-order cleavage rate constants (derived from the human system), k_3, k_5, and k_6 for comparison (*16*−*18*, *20*). The first-order cleavage rate constants utilized in the model were established through iterative analysis of the correlation between experimentally determined cofactor inactivation profiles using 200 nM bovine factor Va and 10 nM APC, and modeled cofactor activity data derived according to the calculation outlined under Methods. The published estimations of cleavage rate constants are all derived from simple exponential fitting to initial rate values from inactivation reactions. Thus, these estimations are presented as second-order rate constants. Our utilization of true cleavage rate constants (k_3, k_5, and k_6) within the model eliminates the possibility of a direct comparison to literature values for the cleavage rate. However, through transformation of our first-order cleavage rate constants (k_{cat}) into pseudo-second-order constants, using the defining relationship k_{cat}/K_m, we are able to compare (approximately) the values utilized in the model and the published values. In our calculation of pseudo-second-order rate values, K_m was approximated by K_d using the rate relationship $K_d = k_2/k_1 = K_m$, and the values of k_3, k_5, and k_6 were utilized as approximations of k_{cat}. These predictions of the observed second-order rate constant are displayed to ease comparison with the commonly reported second-order rate constants k_{cat}/K_m. In comparing these values, it is important to appropriately critique the literature estimations of cleavage rate. The utilization of activity profiles in estimating cleavage rate constants represents the only accessible experimental pathway to these values; however, activity measurements are a poor measure of rate processes for a number of reasons. (1) The measure of activity overtly influences the assembly of factor Va; i.e., factor Xa is known to inhibit the inactivation of factor Va by APC through protecting factor Va either from cleavage or from dissociation. (2) The measure of activity is a slow process (minutes) during which ongoing rate processes such as APC cleavage or fragment dissociation continue at unknown rates. Due to these considerations, the published rate constants are likely to be low approximations of their true value, as illustrated in Table 1.

The model as shown in Figure 6 is most easily interpreted by following the arrows starting in the lower left-hand corner of the cubic representation. The association between intact factor Va and APC (governed by k_1) (eq 6) leads to the formation of the initial enzyme complex (APC·Va) (eq 7). Once formed, this complex may either dissociate (k_2) or proceed through a cleavage event occurring at either Arg^{506} or Arg^{306} (eqs 6, 7); the partitioning of the reactants down these two alternate kinetic pathways is dictated strictly by the individual cleavage rate constants. The cleavage rate constant at $Arg^{662/679}$ (bovine/human) is much lower (<1%) than that for cleavage at either Arg^{306} or Arg^{506}, and has not been observed to affect cofactor activity. Thus, a contribution from this pathway in initial cleavage is omitted from the computational model (note eq 11 is lacking terms including k_6) (*12*, *16*, *18*). Although initial cleavage at Arg^{662} is not included, secondary cleavages at Arg^{662} are included due to their expected influence on the product distribution at extended reaction times (eqs 10, 13, 16). The absence of this initial cleavage pathway in our computational model is not intended to suggest its absence in certain experimental situations but was used to simplify the mathematics.

After the initial cleavage event (eqs 6, 7, 10, 13) (Table 2), the singly cleaved product complex (Va_5·APC or Va_3·APC) either is partitioned to a secondary cleavage reaction or is allowed to dissociate, generating free cleaved factor Va and APC, through the equilibrium governed by k_1, k_2. Cleavage within the singly cleaved species produces the doubly cleaved product complexes: $Va_{5\,3}$·APC, $Va_{5\,3}$·APC, $Va_{3\,6}$·APC, and $Va_{5\,6}$·APC (governed by k_3, k_5, k_6, and eqs 9, 10, 12, 13, 15, 16, 18, 19, 21, 22). The doubly cleaved complex, as before for the singly cleaved product complex, may undergo either dissociation or quaternary cleavage, resulting in the ultimate product, $Va_{5\,3\,6}$·APC (upper right corner of the cube, Figure 6) (eqs 15, 16, 18, 19, 21, 22). The dissociation reaction would again generate the free doubly cleaved factor Va species and free APC; this process is modeled (see Table 2: eqs 15, 16, 18, 19, 21, 22, 24, 25, 35) but is not illustrated in Figure 6 for either the doubly or

the triply cleaved species to reduce the complexity of the figure.

The right edge of the cube illustrates the A2 dissociation processes affecting Arg^{306}-cleaved species, as demonstrated previously and quantitated in the present study (*27*). All complexes in which cleavage at Arg^{306} has occurred are represented on the right-hand face of the cube (shaded in Figure 6). These species have been modeled to dissociate into APC·LC·A1 + HCF (heavy chain fragments) consisting of $A2_C$, $A2_N$, and $A2_{peptide}$ (eqs 12, 13, 15, 16, 18, 19, 24, 25, 27, 28, 31−34). The dissociation reaction of Arg^{306}-cleaved species is governed kinetically by k_7 (this work) and k_8 and is in correspondence to the prior observation detailing dissociation upon cleavage in the presence of lipids, i.e., Arg^{306} (*27*). For simplicity, all of the dissociated species are represented as APC·LC·A1 + HCF; however, each separate species (derived from the corner of the facing cube) independently undergoes the two processes shown along the bottom edge. (1) Dissociation reactions yield free APC and the LC·A1 complex and; (2) association between the appropriate HCF and the LC·A1 complex will yield the corresponding associated cleaved factor Va species according to the association/dissociation equilibrium dictated by k_7, k_8.

To appropriately model the effect of added LC (product inhibition), it is necessary to include terms describing the binding equilibrium between the factor Va HC and LC, described by k_9 and k_{10} (eqs 6, 8, 9, 11, 12, 14, 15, 17, 18, 20, 21, 23, 24, 26, 29, Table 2). Thus, each free factor Va species is modeled to distribute between associated (and thus active) HC·LC and the dissociated products. These equilibria are not illustrated in Figure 6; however, they are included in the model (Table 2). Based upon the previously observed binding interaction being between the LC and APC (*25*, *26*), and the observation that binding between APC and the LC or intact factor Va is indistinguishable (*26*), it was necessary to model the binding interaction between APC and all LC-containing species (e.g., LC·A1) (eqs 29, 30, 35, Table 2). Although the model discriminates between the free LC generated by factor Va dissociation and the LC·A1 complex generated through dissociation of the Arg^{306}-cleaved material, the distribution of these products in terms of their APC binding ability is identical, and thus each is governed by k_1 and k_2. The line along the bottom of Figure 6 describes the interaction between the dissociated free A1·LC species and APC (demonstrated in this work) which yields the A1·LC·APC complex. This interaction is also modeled for the LC generated from factor Va dissociation (see Table 2), but is not illustrated in Figure 6. It is this interaction, A1·LC + APC ↔ A1·LC·APC (as well as the small LC contribution from the association/dissociation equilibrium governed by k_9, k_{10}), which imparts upon the model the product inhibition properties shown experimentally.

Starting in the lower left position of Figure 6, each edge of the cube represented will generate one of the possible mechanistic pathways for the inactivation of factor Va. The heavy arrows tracing one edge of the cube in Figure 6 identify the predominant kinetic pathway predicted from computer simulations (results discussed below). Figure 7 illustrates a theoretical (calculated) reaction progress diagram in terms of substrate utilization and product formation derived from the model at initial conditions of 200 nM factor Va and 10 nM APC and assuming lipid-mediated reaction rates.

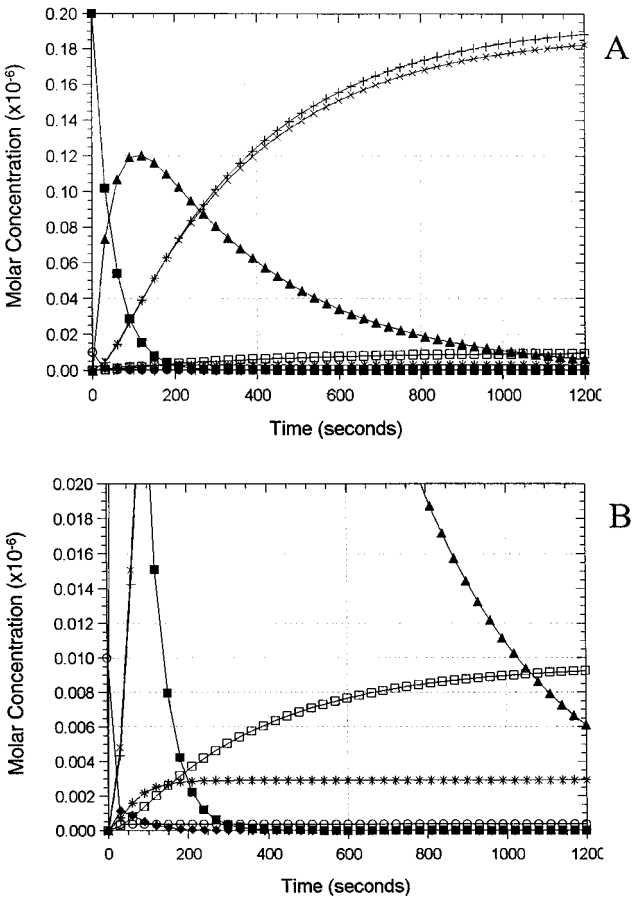

FIGURE 7: Computer simulation of factor Va inactivation: reaction progress diagram. The computer model was seeded with initial conditions of 200 nM factor Va and 10 nM APC and the reaction progress calculated over time in terms of product concentration (for a complete description of this complicated figure, please refer to Results). The symbols are as follows: intact factor Va (■); factor Va_5 (506 cleaved Va) (▲); factor $Va_{5\,3}$ (506/306 cleaved Va) (◆); LC·A1 (×); Va_{A53} ($A2_N$·$A2_C$) (+); LC·APC (□); Va_3 (306 cleaved Va) (●); and Va_{A3} (A2) (*). Panel A illustrates reaction products at concentrations from 20 to 200 nM; panel B illustrates those products at concentrations between 2 and 20 nM. (A) This panel illustrates the major species predicted to occur during factor Va inactivation; prominent initial cleavage consuming Va and generating the species Va_5 and the accumulation of the free LC·A1 species as well as the dissociated Va_{A53} domain are illustrated. (B) This panel predominantly illustrates the lack of initial cleavage at Arg^{306} (Va_3), the short lifetime of the cleaved associated species $Va_{5/3}$, and the prominent accumulation of the LC·APC complex (product inhibition).

The following reaction species concentrations (in μM) are shown during the reaction progress: Va, Va_5, $Va_{5\,3}$, Va_3, LC·A1, APC·LC·A1, APC, Va_{A3} (A2), and $Va_{A5\,3}$ ($A2_N$·$A2_C$). The figure is divided into two panels, A and B. Panel A illustrates the reaction substrates and products at concentrations between 0 and 200 nM. Panel B illustrates the reaction components at concentrations between 0 and 20 nM. Terms accounting for the terminally cleaved dissociated A2 domain products ($Va_{3,5,6} \rightarrow A2_N$·$A2_C$+$A2_{C-peptide}$) are included in the model but are not illustrated in either panel due to their low concentrations ($\ll$2 nM). The low level of these products further demonstrates the lack of influence of Arg^{662} cleavage. Although cleavage at Arg^{662} is not allowed as a primary cleavage and thus cannot influence the early reaction progress, the lack of its influence at longer time points (i.e., 10−20 min, when all factor Va is cleaved at least once and

thus available for cleavage at Arg^{662}) illustrates that this cleavage does not occur on a biologically significant time scale and is therefore not likely to play a predominant role in the APC-dependent inactivation of factor Va.

In panel A, factor Va (■) is shown to be rapidly consumed (within 300 s) predominantly through initial cleavage at Arg^{505} producing the intermediate Va_5 (▲) (Figure 7A). Cleavage of the intermediate Va_5 (▲) at Arg^{306} generates the species $Va_{5\,3}$ (◆) (panel B). The low levels predicted for this product are due to its rapid consumption through dissociation of the cleaved A2 domain, $A2_N{\cdot}A2_C$, generating the LC·A1 complex (×) (panel A) and the free $A2_N{\cdot}A2_C$ species ($Va_{5\,3}$) (+) (panel A). The $Va_{5\,3}$ species may be further cleaved at Arg^{662}, producing $Va_{5\,3\,6}$; however, the rate of $A2_N{\cdot}A2_C$ dissociation (as determined by light scattering analyses) far exceeds the best approximation available for the cleavage rate at Arg^{662}, resulting in dissociation of the factor $Va_{5\,3}$ species prior to this cleavage event. Thus, the product ($Va_{5\,3\,6}$) is not illustrated and would not appear on the chart (panel B) given the scale utilized. Approximately 3% of factor Va is processed through initial cleavage at Arg^{306} producing Va_3 (●) (panel B); as observed for $Va_{5\,3}$, this product dissociates rapidly into the LC·A1 complex (×), panel A, and the intact A2 domain (Va_{A3}*), panel B. Thus, initial cleavage at Arg^{306} is predicted to occur at a very low level, and detection of the resulting products is difficult given the sensitivity of our current techniques (Western blotting). This prediction corresponds well with the collection of published data reporting low levels of the Va_3 product during APC inactivation reactions using catalytic concentrations of APC (*25*, *26*). In Figure 7 the species LC·A1 (×) represents the sum total concentration of all free LC species, nearly all of which (<98%) is derived from cleaved dissociated products; however, a minor component is derived from the association/dissociation equilibrium between the HC and LC. As the reaction progresses, the large pool of LC·A1 species begins to sequester a substantial (>95%) portion of the free APC into APC·LC·A1 complexes (□), panel B. Within 3 min over half of the APC initially available is bound in the nonproductive APC·LC·A1 complex (□), panel B. This prediction is entirely consistent with our observations concerning the LC inhibition of APC.

Predicted Factor Va Cofactor Activities. The product concentration profiles shown in Figure 7 were utilized to calculate theoretical cofactor activity profiles according to the scheme outlined under Methods (eqs 8, 9). Figure 8 (panel A) depicts the predicted factor Va cofactor activity during the time course of inactivation of 200 nM factor Va with 10 nM APC. If the DAPA assay were used at saturating factor Xa, the cleavage-dependent cofactor inactivation would be expected to look like the lower profile (eq 8) (●) while dissociation-dependent cofactor inactivation is predicted by the upper profile (eq 9) (×). The cofactor activity profile expected using a clotting assay (▲) was derived simply by assuming that initial cleavage at Arg^{505} is sufficient to effect complete cofactor inactivation in this assay. The obvious difference between the two methods of cofactor activity assessment (clotting activity vs prothrombinase activity under saturating factor Xa levels) corresponds well with experimental data detailing this assessment (*12*).

The predicted cofactor activity obtained during the inactivation of factor Va^{LEIDEN} (200 nM) with APC (10 nM) is illustrated in Figure 8 (panel C) using notation identical to that described for panel A (●, cleavage-dependent DAPA activity; ×, dissociation-dependent DAPA activity; ▲, clotting activity). Due to the elimination of the Arg^{506} cleavage site, the clotting assay activity now reflects the cleavage-dependent inactivation profile of the DAPA assay since each

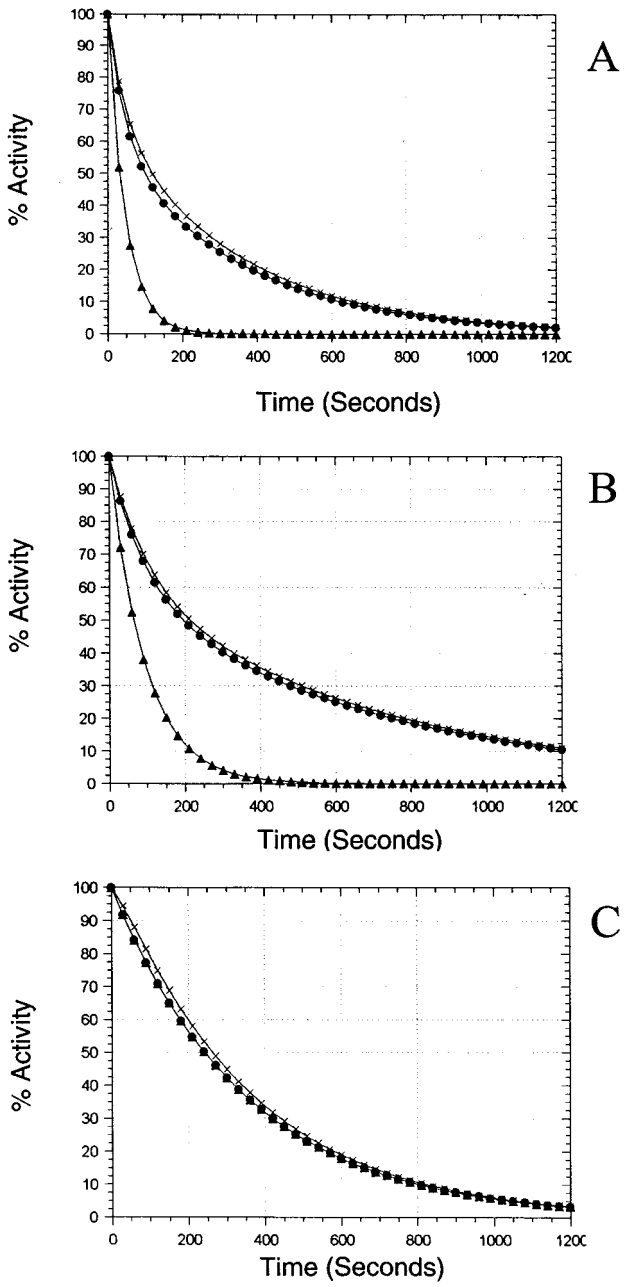

FIGURE 8: Simulated factor Va inactivation: product cofactor activity profile. Panel A: the predicted product cofactor activity obtained upon the inactivation of 200 nM factor Va with 10 nM APC as modeled using the kinetic model and calculated according to Methods is displayed. A simple calculation was made to derive the expected clotting assay cofactor activity through assuming cleavage at Arg^{505} inactivates the cofactor. The expected clotting activity (▲) is compared to the cleavage (●) dependent and dissociation (×) dependent models of cofactor inactivation. Panel B: the predicted product cofactor activity obtained upon the inactivation of 200 nM factor Va with 10 nM APC in the presence of 200 nM free LC is illustrated using the notation as in panels A and B. Panel C: the predicted product cofactor activity obtained upon the inactivation of 200 nM factor Va^{LEIDEN} with 10 nM APC is shown. All activity calculations and figure notations are as detailed in panel A.

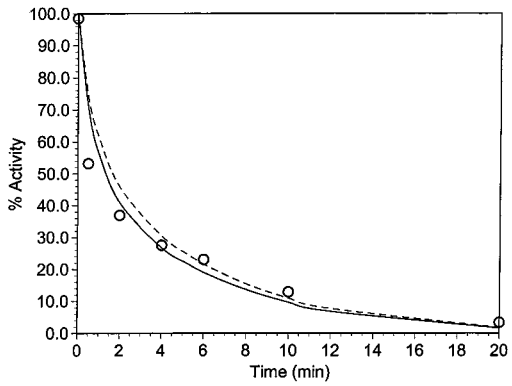

FIGURE 9: Comparison between the simulated cofactor inactivation profile and experimental data. The simulated cofactor inactivation profiles for both cleavage (solid line, shown as ● in Figure 8) and dissociation (dashed line, shown as × in Figure 8) dependent inactivation of factor Va using 200 nM factor Va, 100 μM PC/PS, and 10 nM APC are displayed. The experimental data obtained using the same conditions are shown as open circles (○). The product concentration profiles were used in calculation of the expected cofactor activities according to Methods and are shown as both cleavage (solid line) and dissociation (dashed line) dependent inactivation.

assay system now measures Arg^{306} cleavage only. Comparison between panels A and C demonstrates a relatively minor delay in inactivation (compare DAPA assay activities in each panel) in correlation with numerous experimental findings (*17*, *19*, *54*, *55*). A comparison between the clotting activity found in panels A and C demonstrates a significant delay in the inactivation of factor Va^{LEIDEN} due to the assay sensitivity to cleavage at Arg^{506} in normal factor Va. These results are also in concert with numerous experimental determinations of APC "resistance" ratios in plasma clotting assays and factor V^{LEIDEN} detection. The difference illustrated between panels A and C (▲) quantitatively demonstrates the mechanistic basis for and assay dependence of the APC resistance ratio patient screening assay (*54*, *55*).

Further evaluation of the fitness of the model in predicting cofactor activity profiles was undertaken through evaluation of the effect of the addition of equimolar free LC to the simulation of factor Va (200 nM) inactivation by APC (10 nM). Figure 8 (panel B) illustrates the predicted cofactor activities. The notations used in panels A and C are extended to panel B. Comparison of panels A and B demonstrates a significant delay in the factor Va inactivation process in the presence of excess LC. Furthermore, the delay in both the clotting and DAPA activity profiles demonstrates a generalized inhibition of all cleavage rates (not a specific inhibition as shown in panel C). Inspection of the reaction product profiles for this simulation (as in Figure 7 for normal factor Va) confirmed this assessment and demonstrated that a significant fraction of the added APC (10 nM) was partitioned into the excess LC pool (depleting the available APC for cleavage reactions) (data not shown).

The empirical correlation between the predicted cofactor activity (upper two curves in Figure 8) and the experimentally determined cofactor activity in the DAPA assay at high factor Xa concentrations is shown in Figure 9. The dashed and solid lines correspond to the dissociation- and cleavage-dependent activities, respectively (detailed in Figure 8). The open circles (○) are experimentally derived cofactor activity data using the DAPA assay; 200 nM bovine factor Va and 100 μM PC/PS were treated with 10 nM APC, and the cofactor activity was monitored over time. The predicted cofactor inactivation lines fall on top of the experimentally derived activity measurements, indicating the predictive value of each model.

DISCUSSION

Adequate description of the inactivation of factor Va can be accomplised using a random kinetic cleavage scheme that accounts for product dissociation and the accumulation of APC binding LC-associated products. The necessary inclusion of these processes in understanding (modeling) the inactivation of factor Va results in a complex set of binding equilibria, proteolytic rates, and product dissociation reactions. Previous analysis of this reaction using simplified models has led to a semiquantative understanding of the product dissociation rate, cleavage rates, bond cleavage sites, and their individual effects on cofactor activity. However, the use of activity measurements in attempting to understand the mechanism of factor Va inactivation has produced controversy because the differing assay conditions employed produce different estimates of the relative activities of the various intermediates. The present study shows that adequate kinetic description also requires the inclusion of product inhibition terms resulting from the APC/LC binding interaction. Our enhanced understanding of these complexities, in addition to resolving the discord in understanding this reaction, reduces the utility of simple models of the inactivation reaction which will yield apparently paradoxical effects due to the lack of consideration of product inhibition and product dissociation. In an attempt to clarify the inactivation reaction, we have examined the relationship between bond cleavage and measurable changes in the macromolecular structure of factor Va particularly with respect to product dissociation and rates of inactivation. These results when included with peptide bond cleavage rates and product inhibition have been combined to provide a comprehensive kinetic model that describes the inactivation reaction in rigorous quantitative terms.

The use of light scattering to monitor the macromolecular dissociation of factor Va fragments during inactivation by APC allows for determination of the molecular weight of the membrane-bound and dissociated components, and provides the opportunity to assess changes in factor Va structure as a consequence of cleavage by APC. The data allow estimation of both the rate, 0.028 s^{-1}, of dissociation and the molecular weight (M_r 53 000) of the dissociated product. Furthermore, these data demonstrate that product dissociation plays a contributory role in the inactivation of factor Va, a process homologous to the spontaneous dissociation of the A2 domain of thrombin-activated factor VIIIa (*56*). Evaluation of the kinetics of factor Va A2 domain dissociation upon APC cleavage using light scattering methodologies establishes the dissociation event as occurring coincidentally with cleavage at Arg^{306} as monitored in prothrombinase activity assays. Thus, there exists a high probability that the cleaved associated ($Va_{5\,3}$) cofactor retains a significant level of cofactor activity which is then lost upon dissociation. This has been experimentally demonstrated (*27*). The analysis of the molecular weight change of protein vesicle complexes utilizing light scattering under dynamic reaction conditions is a powerful tool and one which should

be broadly applicable to the generalized study of particle-bound macromolecular association/dissociation reactions (*50*, *51*, *53*, *57*−*59*).

The LC of factor Va is necessary and sufficient to provide tight (nanomolar) binding to APC in the presence of lipids; the strength of this binding interaction is unaffected by the presence or absence of the HC (*26*). Our experimental observation that either the end products of factor Va inactivation or the isolated LC (of either M_r 72 000 or 74 000) can inhibit the inactivation of factor Va confirms that proteolyzed LC complexes will bind APC with a similar affinity to that for free LC or factor Va. Independent of association state, and arguments about the relative activity of cleaved/associated and cleaved/dissociated products, APC-cleaved LC complexes act as APC inhibitors by sequestering the enzyme, APC, into "dead-end" complexes with product. This activity exerts a substantial influence over both the rate and extent of the inactivation reaction and likely accounts for the significant tailing observed in most factor Va inactivation profiles.

The factor Va inactivation process, when observed experimentally, is a predominantly ordered cleavage process, with the first cleavage at Arg^{505} followed by cleavage at Arg^{306}. There has been some question as to the origin of these observations, i.e., the mechanistic pathway. The modeled reaction accounts for these observations based upon a random cleavage process and predicts a small (∼3%) processing of the HC through initial cleavage at Arg^{306} (Figure 7). This prediction is dependent upon the ratio of the cleavage rate constants, k_3 and k_5, and accounts for the scattered experimental observations reporting initial cleavage at Arg^{306} (*17*). Depending upon the method of detection, the observation of products derived from initial cleavage at Arg^{306} can be detected, especially in factor Va molecules resistant to cleavage at the Arg^{505} site (human Arg^{506} as in factor V^{LEIDEN}) (*16*, *19*, *60*). The fact that the kinetic model which allows random cleavage produces substantially a ordered profile (505→306→662; in the human system, 506→306→679) demonstrates that the experimentally observed cleavage pattern is a function of the individual bond cleavage rates and not the fundamental availability of sites for cleavage (*1*, *12*, *19*, *55*, *60*−*62*). Thus, experimental conditions that affect individual bond cleavage rates (such as lipid systems) would be predicted to influence the observed cleavage order and obtained activity profile. Utilizing the kinetic model to generate hypothetical factor Va activity profiles during simulated APC inactivation reactions and comparison of these profiles to experimentally derived data (utilizing anionic lipid membranes) produce modeled cofactor inactivation profiles which nearly overlay with experimental data and confirm the fitness of the computational model. This is further demonstrated in the ability of our computational model to "predict" the known differences in quantitative activity assessment between clotting activity assessment and prothrombinase complex assays.

The importance of factor V^{LEIDEN} as a thrombotic risk factor has been reiterated numerous times in the literature. The fact that factor V^{LEIDEN} afflicts 2−4% of the general population, constitutes the single greatest known risk factor for thrombotic disease, and accounts for up to 50% of the afflicted individuals in familial thrombotic cases argues strongly for the need to understand the mechanistic and kinetic basis for the observed APC resistance. The presented data demonstrate that factor V^{LEIDEN} can be rationally explained solely through the kinetic consequences of elimination of the Arg^{506} (Arg^{505} bovine) cleavage site within a random model of factor Va inactivation. The demonstrated correspondence between the modeled and experimental data in the case of normal and factor V^{LEIDEN} inactivation does not de novo demonstrate the existence of a random cleavage mechanism. However, the combination of these results and the observations made on the effect of exogenous LC addition together provide firm evidence in support of a random cleavage mechanism as modeled here.

The present extension of the prior observation that APC binds equally well to factor Va and free LC (*26*) leads to the functional studies shown in this report and establishes the LC and its associated complexes as important mediators of the rate and extent of factor Va inactivation. The correspondence between the predictive model system in demonstrating LC inhibition of APC and the experimental data demonstrating extensive inhibition of factor Va inactivation by both purified LC species and the reaction products associated with APC cleavage of factor Va (A1·LC) demonstrates conclusively the importance of this process. The in vivo circulating half-life of the LC has been measured in a baboon model where it was found to be removed from circulation rapidly (*63*). However, the ultimate cause for the observed rapid clearance of the LC in this or other in vivo models is unknown, and the possibility that this species is sequestered onto the endothelial lining due to its lipid binding properties suggests that a substantial pool of APC inhibitory potential (free LC and LC complexes) may exist on the lumen of the vascular circulation. Experiments designed to assess the fate and inhibitory potential of this species may prove to be quite informative with respect to the physiology of factor Va inactivation.

The correlation between the observed light scattering traces and the cofactor inactivation profiles suggests that cleaved associated factor Va species, in particular the kinetically predominant reaction product $Va_{5\,3}$, maintain cofactor activity until undergoing spontaneous dissociation ($k = 0.028\ s^{-1}$). The ability to experimentally discern this difference in activity between cleaved and associated products and their dissociated species is limited due to the measured half-life (35 s) of the associated cleaved cofactor. In other work we have demonstrated 20% residual activity in totally cleaved factor Va (after 3 min of cleavage, i.e., 5 half-lives) under saturating factor Xa conditions, establishing a lower limit to the functional activity of this species (*27*). This interpretation is somewhat complicated by cleavage rate considerations and thus the relatively uncertain concentration of the associated species. However, the high level of sequence homology and structural domain organization between APC-cleaved factor Va and thrombin-activated factor VIIIa is in support of the hypothesis of dissociation-dependent inactivation. The reported spontaneous inactivation of factor VIIIa following thrombin activation (Arg^{372}) occurs through dissociation of the VIIIa A2 domain at a rate of $0.005\ s^{-1}$ (*56*), although this rate is substantially dependent upon solution conditions (pH among others). Using light scattering analysis, we have determined the rate of spontaneous dissociation of the APC-cleaved factor Va A2 domain as $0.028\ s^{-1}$. The fact that

cleaved factor Va dissociates approximately 6 times faster than factor VIIIa at physiologic conditions indicates that Arg^{306}-cleaved factor Va is much less stable than factor VIIIa. The observation that dissociation of APC-cleaved factor Va is largely irreversible at any concentration whereas factor VIIIa is relatively stable at higher concentrations is probably a function of the equilibrium constant defining the dissociation reaction (*64*). The reported dissociation constant for the A2 domain of thrombin-activated factor VIIIa is 28−200 nM (*64*) while the value for factor Va can only be estimated as greater than 10 μM (*27*). Thus, a measurement of the activity associated with associated cleaved factor $Va_{5\,3}$ may be impossible through direct means; however, all the data and corollary systems suggest that it is likely to be significant and that inactivation will be mediated principally through dissociation.

ACKNOWLEDGMENT

We thank Drs. Sriram Krishnasawamy and Michael Nesheim for their valuable discussions on the use of light scattering in analyzing protein−lipid interactions and their suggestions in mathematical derivation, Dr. Richard Jenny of Hematologic Technologies for the generous gift of bovine factor Xa and APC, Dr. Walter F. Stafford III for his willingness to discuss the $g(s^*)$ analyses and their appropriate manipulation, Ted Foss for writing the software "Max-Fit", and Laura Rounds for her technical assistance in the electron microscopic analyses.

REFERENCES

1. Kalafatis, M., Rand, M. D., and Mann, K. G. (1994) *J. Biol. Chem. 269*, 31869−31880.
2. Mann, K. G., Nesheim, M. E., Church, W. R., Haley, P., and Krishnaswamy, S. (1990) *Blood 76*, 1−16.
3. Kalafatis, M., Egan, J. O., van't Veer, C., Cawthern, K. M., and Mann K. G. (1997) *Eukaryotic Gene Expression 7*, 241−280.
4. Nesheim, M. E., Taswell, J. B., and Mann, K. G. (1979) *J. Biol. Chem. 254*, 10952−10962.
5. Nesheim, M. E., and Mann, K. G. (1979) *J. Biol. Chem. 254*, 1326−1334.
6. Nesheim, M., Kettner, C., Shaw, E., and Mann, K. G. (1981) *J. Biol. Chem. 256*, 6537−6540.
7. Suzuki, K., Dahlback, B., and Stenflo, J. (1982) *J. Biol. Chem. 257*, 6556−6564.
8. van Dieijen, G., Tans, G., Rosing, J., and Hemker, H. C. (1981) *J. Biol. Chem. 256*, 3433−3442.
9. Krishnaswamy, S., Field, K. A., Edgington, T. S., Morrissey, J. H., and Mann, K. G. (1992) *J. Biol. Chem. 267*, 26110−26120.
10. Krishnaswamy, S., and Mann, K. G. (1988) *J. Biol. Chem. 263*, 5714−5723.
11. Tracy, P. B., Peterson, J. M., Nesheim, M. E., McDuffie, F. C., and Mann, K. G. (1979) *J. Biol. Chem. 254*, 10354−10361.
12. Kalafatis, M., and Mann, K. G. (1993) *J. Biol. Chem. 268*, 27246−27257.
13. Esmon, C. T., and Owen, W. G. (1981) *Proc. Natl. Acad. Sci. U.S.A. 78*, 2249−2252.
14. Esmon, N. L., Owen, W. G., and Esmon, C. T. (1982) *J. Biol. Chem. 257*, 859−869.
15. Owen, W. G., and Esmon, C. T. (1981) *J. Biol. Chem. 256*, 5532−5535.
16. Egan, J. O., Kalafatis, M., and Mann, K. G. (1997) *Protein Sci. 6*, 2016−2027.
17. Nicolaes, G. A. F., Tans, G., Thomassen, M. C. L. G. D., Hemker, H. C., Pabinger, I., Varadi, K., Schwarz, H. P., and Rosing, J. (1995) *J. Biol. Chem. 270*, 21158−21166.
18. Hockin, M. F., Kalafatis, M., Shatos, M. A., and Mann, K. G. (1997) *Arterioscler. Thromb. Vasc. Biol. 17*, 2765−2775.
19. Kalafatis, M., Bertina, R. M., Rand, M. D., and Mann, K. G. (1995) *J. Biol. Chem. 270*, 4053−4057.
20. Rosing, J., Hoekema, L., Nicolaes, G. A. F., Thomassen, M. C. L. G. D., Hemker, H. C., Varadi, K., Schwarz, H. P., and Tans, G. (1995) *J. Biol. Chem. 270*, 27852−27858.
21. Jenny, R. J., Pittman, D. D., Toole, J. J., Kriz, R. W., Aldape, R. A., Hewick, R. M., Kaufman, R. J., and Mann, K. G. (1987) *Proc. Natl. Acad. Sci. U.S.A. 84*, 4846−4850.
22. Guinto, E. R., Esmon, C. T., Mann, K. G., and MacGillivray, R. T. A. (1992) *J. Biol. Chem. 267*, 2971−2978.
23. Esmon, C. T. (1979) *J. Biol. Chem. 254*, 964−973.
24. Krishnaswamy, S., Russell, G. D., and Mann, K. G. (1989) *J. Biol. Chem. 264*, 3160−3168.
25. Kalafatis, M., Rand, M. D., and Mann, K. G. (1994) *Biochemistry 33*, 486−493.
26. Krishnaswamy, S., Williams, E. B., and Mann, K. G. (1986) *J. Biol. Chem. 261*, 9684−9693.
27. Mann, K. G., Hockin, M. F., Begin, K. J., and Kalafatis, M. (1997) *J. Biol. Chem. 272*, 20678−20683.
28. Odegaard, B., and Mann, K. (1987) *J. Biol. Chem. 262*, 11233−11243.
29. Lawson, J. H., Kalafatis, M., Stram, S., and Mann, K. G. (1994) *J. Biol. Chem. 269*, 23357−23366.
30. Jones, K. C., and Mann, K. G. (1994) *J. Biol. Chem. 269*, 23367−23373.
31. Nesheim, M. E., Tracy, R. P., and Mann, K. G. (1984) *J. Biol. Chem. 259*, 1447−1453.
32. Gentry, R., Liqiang, Y., and Nemerson, Y. (1997) *Biophys. J. 69*, 362−371.
33. Bauer, K. A., and Griffin, J. H. (1995) *N. Engl. J. Med. 332*, 1383.
34. Catto, A., Carter, A., Ireland, H., Bayston, T. A., Philippou, H., Barrett, J., Lane, D. A., and Grant, P. J. (1995) *Arterioscler. Thromb. Vasc. Biol. 15*, 783−785.
35. Bertina, R. M., Koeleman, B. P. C., Koster, T., Rosendaal, F. R., Dirven, R. J., de Ronde, H., van der Velden, P. A., and Reitsma, P. H. (1994) *Nature 369*, 64−67.
36. Koster, T., Rosentaal, F. R., de Ronde, H., Brie, T. E., Vandenbroucke, J. P., and Bertina, R. M. (1992) Venous thrombosis due to poor anticoagulant response to activated protein C: the Leiden thrombophilia study. *Lancet 342*, 1503−1506.
37. Rees, D. C., Cox, M., and Clegg, J. B. (1995) *Lancet 346*, 1133−1134.
38. Kalafatis, M., Lu, D., Bertina, R. M., Long, G. L., and Mann, K. G. (1995) *Arterioscler. Thromb. Vasc. Biol. 15*, 2181−2187.
39. Nesheim, M. E., Katzmann, J. A., Tracy, P. B., and Mann, K. G. (1981) in *Methods in Enzymology, Proteolytic Enzymes, Part C* (Lorand, L., Ed.) pp 249−285, Academic Press Inc., New York.
40. Katzmann, J. A., Nesheim, M. E., Hibbard, L. S., and Mann, K. G. (1981) *Proc. Natl. Acad. Sci. U.S.A. 78*, 162−166.
41. Kalafatis, M., Krishnaswamy, S., Rand, M. D., and Mann, K. G. (1993) in *Methods in Enzymology, Part A* (Lorand, L., and Mann, K. G., Eds.) pp 224−236, Academic Press, San Diego.
42. Barenholz, Y., Gibbes, D., Litman, B. J., Goll, J., Thompson, T. E., and Carlson, F. D. (1977) *Biochemistry 16*, 2806−2810.
43. Huang, C. (1969) *Biochemistry 8*, 344−352.
44. Newman, G. C., and Huang, C. (1975) *Biochemistry 14*, 3363−3369.
45. Gomori, G. (1942) *J. Lab. Clin. Med. 27*, 955−960.
46. Stafford, W. F. (1992) *Anal. Biochem. 203*, 295−301.
47. Nesheim, M. E., Prendergast, F. G., and Mann, K. G. (1979) *Biochemistry 18*, 996−1003.
48. Doyle, M. F., and Haley, P. E. (1993) *Methods Enzymol. 222*, 299−312.
49. Abbott, A. J., and Nelsestuen, G. L. (1987) *Biochemistry 26*, 7994−8003.
50. Nelsestuen, G. L., and Lim, T. K. (1977) *Biochemistry 16*, 4164−4171.

51. Schwalbe, R. A., Dahlbäck, B., Hillarp, A., and Nelsestuen, G. L. (1990) *J. Biol. Chem. 265*, 16074−16081.
52. Huang, C., and Mason, J. T. (1978) *Proc. Natl. Acad. Sci. U.S.A. 75*, 308−310.
53. Krishnaswamy, S., Jones, K. C., and Mann, K. G. (1988) *J. Biol. Chem. 263*, 3823−3834.
54. Kalafatis, M., and Mann, K. G. (1997) *Arterioscler. Thromb. Vasc. Biol. 17*, 620−627.
55. Kalafatis, M., Haley, P. E., Lu, D., Bertina, R. M., Long, G. L., and Mann, K. G. (1996) *Blood 87*, 4695−4707.
56. Lollar, P., Parker, E. T., and Fay, P. J. (1992) *J. Biol. Chem. 267*, 23652−23657.
57. Nelsestuen, G. L., and Broderius, M. (1977) *Biochemistry 16*, 4172−4177.
58. Wei, G. J., Bloomfield, V. A., Resnick, R. M., and Nelsestuen, G. L. (1982) *Biochemistry 21*, 1949−1959.
59. Kung, C., Hayes, E., and Mann, K. G. (1994) *J. Biol. Chem. 269*, 25838−25848.
60. Heeb, M. J., Kojima, Y., Greengard, J. S., and Griffin, J. H. (1995) *Blood 85*, 3405−3411.
61. van't Veer, C., Golden, N. J., Kalafatis, M., and Mann, K. G. (1997) *J. Biol. Chem. 272*, 7983−7994.
62. Aparicio, C., and Dahlbäck, B. (1996) *Biochem. J. 313*, 467−472.
63. Rand, M. D., Hanson, S. R., and Mann, K. G. (1995) *Blood 86*, 2616−2623.
64. Fay, P. J., and Smudzin, T. M. (1992) *J. Biol. Chem. 267*, 13246−13250.
65. Hockin, M. F., et al. (1997) *Blood 90*, Abstr. 639.

BI981966E